Chapter 5 in the book:
P.A. Kralchevsky and K. Nagayama, "Particles at Fluid Interfaces and Membranes," Elsevier, Amsterdam, 2001; pp. 183–247

CHAPTER 5

LIQUID FILMS AND INTERACTIONS BETWEEN PARTICLE AND SURFACE

The collision of a colloid particle with an interface, or with another particle, is accompanied by the formation of a thin liquid film. The particle(s) will stick or rebound depending on whether repulsive or attractive forces prevail in the liquid film. In the case of an equilibrium liquid film the repulsive forces dominate the disjoining pressure, which is counterbalanced by the action of transversal tension, the latter being dominated by the attractive forces in the transition zone film–meniscus. The Derjaguin approximation allows one to calculate the force across a film of uneven thickness if the interaction energy per unit area of a plane-parallel film is known.

Next we consider interactions of different physical origin. Expressions for the van der Waals interaction between surfaces of various shape are presented. Hypotheses about the nature of the long-range hydrophobic surface force are discussed. Special attention is paid to the electrostatic surface force which is due to the overlap of the electric double layers formed at the charged surfaces of an aqueous film. The effects of excluded volume per ion and ionic correlations lead to the appearance of a hydration repulsion and an ion-correlation attraction. The presence of fine colloidal particles in a liquid film gives rise to an oscillatory structural force which could stabilize the film or cause its step-wise thinning (stratification). At low volume fractions of the fine particles the oscillatory force degenerates into the depletion attraction, which has a destabilizing effect. The overlap of "brushes" from adsorbed polymeric molecules produces a steric interaction. The configurational confinement of thermally excited surface modes engenders repulsive undulation and protrusion forces. Finally, the collisions of emulsion drops are accompanied with deformations, i.e. deviations from the spherical shape. They cause extension of the drop surface area and change in the surface curvature, which lead to dilatational and bending contributions to the overall interaction energy. The total particle–surface (or particle–particle) interaction energy is a superposition of contributions from all operative surface interactions. In addition, hydrodynamic interactions, due to the viscous friction in a liquid film, are considered in the next Chapter 6.

5.1. MECHANICAL BALANCES AND THERMODYNAMIC RELATIONSHIPS

5.1.1. INTRODUCTION

A necessary step in the process of interaction of a colloidal particle (solid bead, liquid drop or gas bubble) with an interface is the formation of a liquid film (Fig. 5.1). For example, a liquid film of uniform thickness can be formed when a fluid particle approaches a solid surface, see Fig. 5.1a. The shape of such a film is circular; the radius of the contact line at its periphery is denoted by r_c . From a geometric (and hydrodynamic) viewpoint a liquid film is termed *thin* when its thickness h is relatively small, viz. $h/r_c << 1$. From a physical viewpoint a liquid film is called *thin* if its thickness is sufficiently small that the molecular interactions between the two adjacent phases across the film are not negligible; as a rule this happens for $h \leq 100$ nm [1]. These molecular interactions across the film are often termed *surface forces* [2,3]. The surface force per unit area of the film is called *disjoining pressure*, Π, [4]. In general, the disjoining pressure depends on the film thickness, $\Pi = \Pi(h)$. Since Π is an excess pressure in the thin liquid film with respect to the bulk liquid, Π vanishes in a *thick* film, that is $\Pi \to 0$ for $h \to \infty$.

The disjoining pressure can be both *repulsive* ($\Pi > 0$) and *attractive* ($\Pi < 0$). A repulsive disjoining pressure may keep the two film surfaces at a given distance apart, thus creating a stable liquid film of uniform thickness, like that depicted in Fig. 5.1a. In contrast, attractive disjoining pressure destabilizes the liquid films. In the case of two solid surfaces interacting across a liquid $\Pi < 0$ leads to adhesion of the two solids. If one of the film surfaces is fluid, the attractive disjoining pressure enhances the amplitude of the thermally excited fluctuation capillary waves, which grow until the film ruptures [5-9], see Section 6.2.

In the case of a solid particle approaching a solid surface, the gap between the two surfaces can be treated as a liquid film of *nonuniform* thickness (Fig. 5.1b). Similar configuration may happen if the particle is fluid, but its surface tension is high enough, and/or its size is sufficiently small.

If the interface is fluid, it undergoes some deformation produced by the interaction with the

approaching particle (Fig. 5.1c). When the liquid film ruptures, one says that the particle "enters" the fluid phase boundary. The occurrence of "entry" is important for the antifoaming action of small oil drops; this is considered in more details in Chapter 14 of this book.

If a particle is entrapped within a liquid film (Fig. 5.1d), two additional liquid films appear in the upper and lower part of the particle surface. Such a configuration is used in the film trapping technique (FTT), which allows one to measure the contact angles of μm-sized particles [10], and to investigate the adhesive energy and physiological activation of biological cells [11,12]. (See also Fig. 5.6 below.)

In this chapter we first derive and discuss basic mechanical balances and thermodynamical equations related to thin liquid films and equilibrium attachment of particles to interfaces (Section 5.1). Next, we consider separately various kinds of surface forces in thin liquid films (Section 5.2). In Chapter 6 we present an overview of the hydrodynamic interactions particle–interface and particle–particle. (Section 6.2).

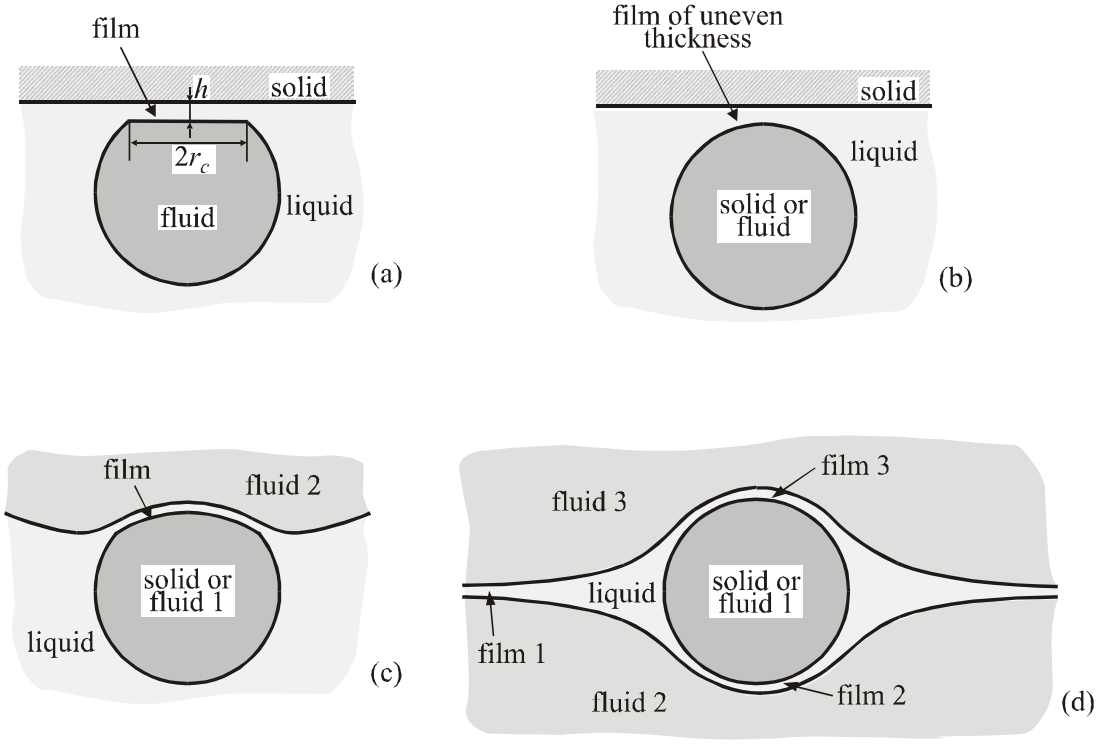

Fig. 5.1. Various configurations particle–interface which are accompanied with the formation of a thin liquid film: (a) fluid particle (drop or bubble) at a solid interface; (b) solid particle at a solid surface; (c) solid or fluid particle at a fluid interface; (d) particle trapped in a liquid film.

5.1.2. DISJOINING PRESSURE AND TRANSVERSAL TENSION

Figure 5.2 shows a sketch of a fluid particle (drop or bubble) which is attached to a solid substrate. At equilibrium (no hydrodynamic flows) the pressure P_l in the bulk liquid phase is isotropic. The pressure inside the fluid particle, P_{in}, is higher than P_l because of the interfacial curvature (cf. Chapter 2):

$$\frac{2\sigma}{R} = P_{in} - P_l \equiv P_c \tag{5.1}$$

where σ is the fluid–liquid interfacial tension, P_c is the capillary pressure (the pressure jump across the curved interface), and R is the radius of curvature. The force balance *per unit area* of the upper film surface (Fig. 5.2) is given by the equation [13]

$$P_{in} = P_l + \Pi(h) \tag{5.2}$$

In other words, the increased pressure inside the fluid particle ($P_{in} > P_l$) is counterbalanced by the repulsive disjoining pressure $\Pi(h)$ acting in the liquid film. For a given $\Pi(h)$-dependence, this balance of pressures determines the equilibrium thickness of the film. The comparison of Eqs. (5.1) and (5.2) shows that at equilibrium the disjoining pressure is equal to the capillary pressure:

$$\Pi(h) = P_c \tag{5.3}$$

Next, let us consider the force balance *per unit length* of the contact line, which encircles the plane-parallel film [14,15]:

$$\underline{\boldsymbol{\sigma}} + \underline{\boldsymbol{\sigma}}^f + \underline{\boldsymbol{\tau}} = 0 \tag{5.4}$$

The vectors $\underline{\boldsymbol{\sigma}}$, $\underline{\boldsymbol{\sigma}}^f$ and $\underline{\boldsymbol{\tau}}$ are shown in Fig. 5.2; σ^f is the tension of the upper film surface, which is different from the liquid–fluid interfacial tension σ (as a rule $\sigma^f < \sigma$), see Eq. (5.5) below. τ is the so called *transversal tension* which is directed normally to the film surface. The transversal tension is a linear analogue of the disjoining pressure: τ accounts for the excess interactions across the liquid film in the narrow *transition zone* between the uniform film and the bulk liquid phase. (Microscopically this transition zone can be treated as a film of uneven thickness and a micromechanical expression for τ can be derived – see Ref. 15.) Note that, in

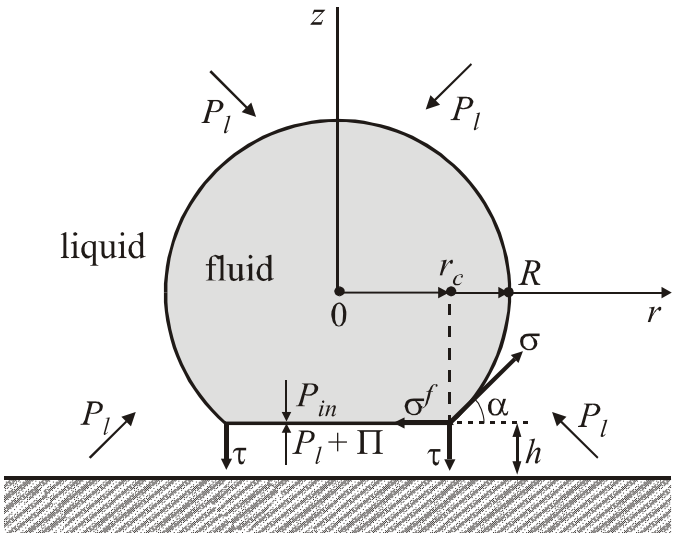

Fig. 5.2. Sketch of a fluid particle which is attached to a solid surface. A plane-parallel film of thickness h and radius r_c is formed in the zone of attachment; P_{in} and P_l are the pressures in the inner fluid and in the outer liquid; Π is disjoining pressure; σ and σ^f are surface tensions of the outer fluid–liquid phase boundary and of the film surface; τ is transversal tension.

general, Eq. (5.4) may contain an additional line-tension term, cf. Eq. (2.73), which is usually very small and is neglected here; see Section 2.3.4 and Eq. (5.31) below. The horizontal and vertical projections of Eq. (5.4) have the form:

$$\sigma^f = \sigma \cos\alpha \tag{5.5}$$

$$\tau = \sigma \sin\alpha \tag{5.6}$$

where α is the contact angle. Since $\cos\alpha < 1$, Eq. (5.5) shows that $\sigma^f < \sigma$. In addition, Eq. (5.6) states that the transversal tension τ counterbalances the normal projection of the surface tension with respect to the film surface.

To understand deeper the above force balances, we will use a thermodynamic relationship,

$$\frac{\partial \sigma^f}{\partial h} = -\Pi\,, \qquad \text{(wetting film)} \tag{5.7}$$

which is derived in the next Section 5.1.3. The integration of the latter equation, along with the

boundary condition $\lim_{h\to\infty} \sigma^f(h) = \sigma$, yields

$$\sigma^f(h) = \sigma + \int_h^\infty \Pi(h)dh \qquad \text{(wetting film)} \tag{5.8}$$

In fact, the integral

$$f(h) \equiv \int_h^\infty \Pi(h)dh \tag{5.9}$$

expresses the work (per unit area) performed against the surface forces to bring the two film surfaces from an infinite separation to a finite distance h; $f(h)$ has the meaning of excess free energy per unit area of the thin liquid film. Comparing Eqs. (5.5) and (5.8) one obtains

$$\cos\alpha = 1 + \frac{1}{\sigma}\int_h^\infty \Pi(h)dh = 1 + \frac{f(h)}{\sigma} \qquad \text{(wetting film)} \tag{5.10}$$

In addition, the combination of Eqs. (5.6) and (5.10) yields

$$\tau = \sigma\left[1 - (1 + f/\sigma)^2\right]^{1/2} \approx (-2f\sigma)^{1/2} \qquad (f/\sigma << 1) \tag{5.11}$$

Equations (5.10) and (5.11) show that the interaction free energy must be negative, that is $f < 0$; otherwise equilibrium attachment of a particle to the interface (Fig. 5.2) is impossible. The condition $f < 0$ is often satisfied because at long distances the integrand $\Pi(h)$ in Eq. (5.9) is negative, which in a final reckoning can give a negative f.

For aqueous films the disjoining pressure is often a superposition of electrostatic repulsion and van der Waals attraction [16,17]:

$$\Pi(h) = C\exp(-\kappa h) - \frac{A_{\mathrm{H}}}{6\pi h^3} \tag{5.12}$$

Here C is a constant, κ is the Debye screening parameter and A_{H} is the Hamaker constant; see Section 5.2 for details. A typical shape of the $\Pi(h)$ dependence, determined from Eq. (5.12), is shown in Fig. 5.3; the portion of the curve on the left of the primary minimum is due to the short-range Born repulsion, which is not accounted for in Eq. (5.12). One sees that the equation $\Pi(h) = P_c$ may have three roots corresponding to three possible equilibrium states the liquid

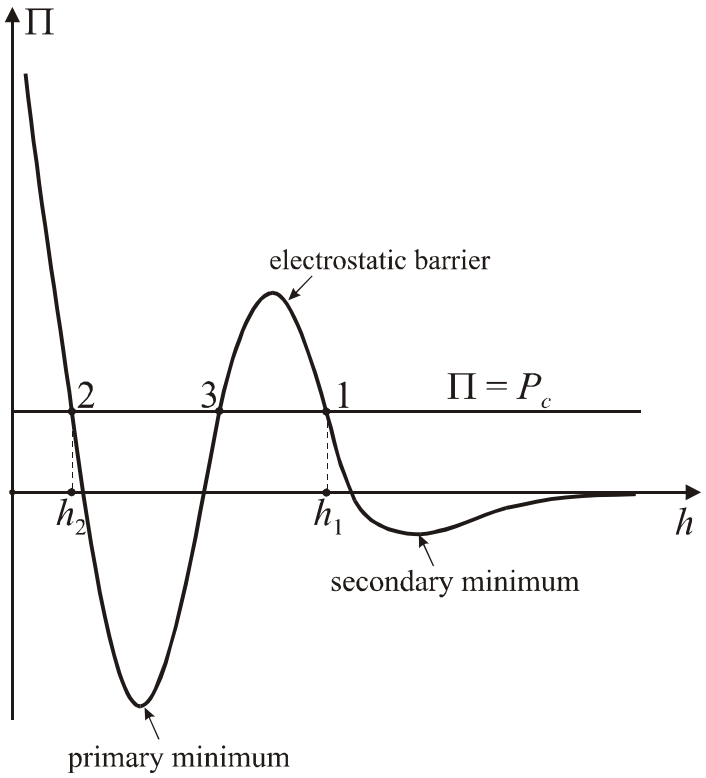

Fig. 5.3. A typical disjoining pressure isotherm, Π vs. h, predicted by Eq. (5.12). The intersection points of the curve Π(h) with the horizontal line Π = P_c correspond to equilibrium states of the film: Points 1 and 2 – stable primary and secondary films; Point 3 – unstable equilibrium state.

film, see Eq. (5.3). Point 1 in Fig. 5.3 corresponds to a film, which is stabilized by the double layer repulsion; sometimes such a film is called the *primary film* or *common black film*. Point 3 corresponds to unstable equilibrium and cannot be observed experimentally. Point 2 corresponds to a very thin film, which is stabilized by the short range repulsion; such a film is called the *secondary film* or *Newton black film*. Transitions from common to Newton black films are often observed with foam and emulsion films [18-21].

As an example, let us assume that the state of the film in Fig. 5.2 corresponds to Point 1 in Fig. 5.3. Then obviously $\Pi(h_1) = P_c > 0$, i.e. the disjoining pressure is *repulsive* and keeps the two film surfaces at an equilibrium distance h_1 apart (film of uniform thickness is formed). On the other hand, the attractive surface forces (the zone of the "secondary minimum" in Fig. 5.3) prevail in the integral in Eq. (5.9). In such case we have $f(h_1) < 0$ and consequently, the contact angle α does exists, see Eq. (5.10), and the transversal tension τ is a real positive quantity, see

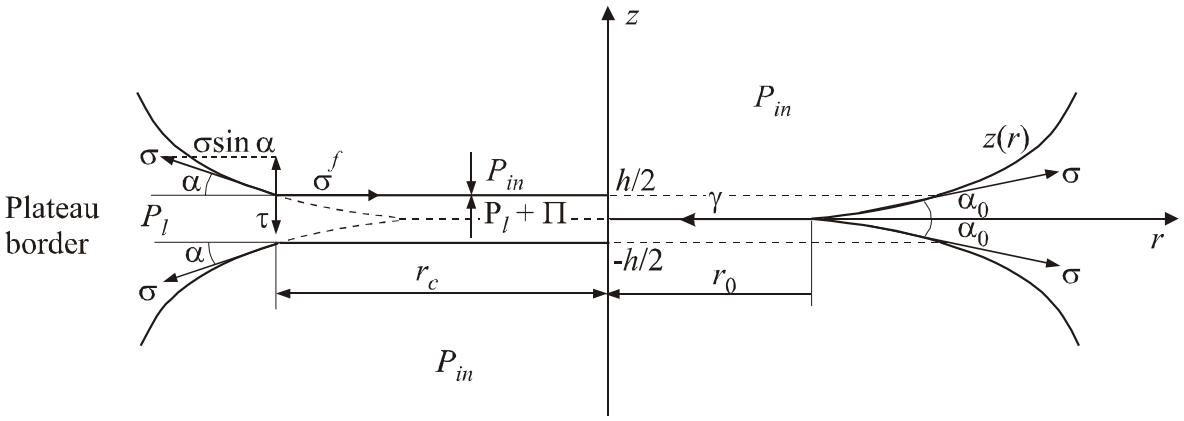

Fig. 5.4. Schematic presentation of the detailed and membrane models of a thin liquid film: on the left- and right-hand side, respectively.

Eq. (5.11). Note that in Fig. 5.2 Π and τ have the opposite directions; indeed, as seen from Fig. 5.3, and Eqs. (5.9) and (5.11), their values are determined by the predominant repulsion (for Π) and attraction (for τ). The fact the directions of Π and τ are opposite has a crucial importance for the existence of equilibrium state of an attached particle at an interface. To demonstrate that let us consider the total balance of the forces exerted on the fluid particle in Fig. 5.2.

If the particle is small (negligible effect of gravity), then the integral of P_l over the surface of the fluid particle in Fig. 5.2 is equal to zero. Then the total balance of the forces exerted on the particle reads [22,23]

$$\pi r_c^2 \Pi = 2\pi r_c \tau \tag{5.13}$$

i.e. the disjoining pressure Π, multiplied by the film area, must be equal to the transversal tension τ, multiplied by the length of the contact line. Thus it turns out that the fluid particle sticks to the solid surface *at its contact line* (at the film periphery) where the long-range attraction (accounted for by τ) prevails; on the other hand, the repulsion predominates inside the film, where $\Pi = P_c > 0$. The exact balance of these two forces of opposite direction, expressed by Eq. (5.13), determines the state of equilibrium attachment of the particle to the interface. Note that the conclusions based on Eq. (5.13) are valid not only for particle–wall attachment, but also for particle-particle interactions, say for the formation of doublets and

multiplets (flocs) from drops in emulsions [24].

For larger particles the gravitational force F_g, which represents the difference between the particle weight and the buoyancy (Archimedes) force, may give a contribution to the force balance in Eq. (5.13), [22,23]:

$$\pi r_c^2 \Pi = 2\pi r_c \tau + F_g, \qquad F_g \equiv \Delta\rho g V_p \tag{5.14}$$

Here $\Delta\rho$ is the difference between the mass densities of the fluid particle and the outer liquid phase, g is the acceleration due to gravity and V_p is the volume of the particle.

5.1.3. THERMODYNAMICS OF THIN LIQUID FILMS

First, we consider symmetric thin liquid films, like that depicted in Fig. 5.4. Since such films have two *fluid* surfaces, the respective thermodynamic equations sometimes differs from their analogues for wetting films (Section 5.1.2) by a multiplier 2; these differences will be noted in the text below. Symmetric films appear between two attached similar drops or bubbles, as well as in foams. As in Fig. 5.2, P_{in} is the pressure in the fluid particles and P_l is the pressure in the outer liquid phase (in the case of foam – that is the liquid in the Plateau borders). The force balances per unit area of the film surface and per unit length of the contact line (see the left-hand side of Fig. 5.4) lead again to Eqs. (5.2)–(5.6).

It should be noted that two different, but supplementary, approaches (models) are used in the macroscopic description of a thin liquid film. These are the "detailed approach", used until now, and the "membrane approach"; they are illustrated, respectively, on the left- and right-hand side of Fig. 5.4. As described above, the "detailed approach" models the film as a liquid layer of thickness h and surface tension σ^f. In contrast, the "membrane approach", treats the film as a membrane of zero thickness and total tension, γ, acting tangentially to the membrane – see the right-hand side of Fig. 5.4. By making the balance of the forces acting on a plate of unit width along the y-axis (in Fig. 5.4 the profile of this plate coincides with the z-axis) one obtains the Rusanov [25] equation:

$$\gamma = 2\sigma^f + P_c h \qquad (P_c = P_{in} - P_l) \tag{5.15}$$

Equation (5.15) expresses a condition for equivalence between the membrane and detailed models with respect to the lateral force.

In the framework of the *membrane approach* the film can be treated as a single surface phase, whose Gibbs-Duhem equation reads [23,25,26]:

$$d\gamma = -s^f dT - \sum_{i=1}^{k} \Gamma_i d\mu_i \tag{5.16}$$

where γ is the film tension, T is temperature, s^f is excess entropy per unit area of the film, Γ_i and μ_i are the adsorption and the chemical potential of the i-th component. The Gibbs-Duhem equations of the liquid phase (l) and the "inner" phase (in) read

$$dP_\chi = s_v^\chi dT + \sum_{i=1}^{k} n_i^\chi d\mu_i, \qquad \chi = l, in \tag{5.17}$$

where s_v^χ and n_i^χ are entropy and number of molecules per unit volume, and P_χ is pressure in the respective phase. Since $P_c = P_{in} - P_l$, from Eq. (5.17) one can obtain an expression for dP_c. Further, we multiply this expression by h and subtract the result from the Gibbs-Duhem equation of the film, Eq. (5.16). The result reads

$$d\gamma = -\widetilde{s}\, dT + h\, dP_c - \sum_{i=1}^{k} \widetilde{\Gamma}_i d\mu_i \tag{5.18}$$

where

$$\widetilde{s} = s^f + \left(s_v^0 - s_v^l\right)h, \qquad \widetilde{\Gamma}_i = \Gamma_i + \left(n_i^0 - n_i^l\right)h, \qquad i = 1,...,k \tag{5.19}$$

An alternative derivation of the same equations is possible, after Toshev and Ivanov [27]. Imagine two equidistant planes separated at a distance h. The volume confined between the two planes is thought to be filled with the bulk liquid phase "l". Taking surface excesses with respect to the bulk phases, one can derive Eqs. (5.18) and (5.19) with $\widetilde{s}$ and $\widetilde{\Gamma}_i$ being the excess surface entropy and adsorption ascribed to the surfaces of this liquid layer. A comparison between Eqs. (5.18) and (5.16) shows that there is one additional term in Eq. (5.18), viz. $h\, dP_c$. It corresponds to one supplementary degree of freedom connected with the

choice of the parameter h. To specify the model one needs an additional equation to determine h. For example, let this equation be

$$\widetilde{\Gamma}_1 = 0 \tag{5.20}$$

Equation (5.20) requires h to be the thickness of a liquid layer from phase "l", containing the same amount of component 1 as the real film. This thickness is called the thermodynamic thickness of the film [28]. It can be of the order of the real film thickness if component 1 is chosen in an appropriate way, say, to be the solvent in the film phase.

Combining Eqs. (5.3), (5.18) and (5.20) one obtains [27]

$$d\gamma = -\widetilde{s}\,dT + h d\Pi - \sum_{i=2}^{k} \widetilde{\Gamma}_i d\mu_i \tag{5.21}$$

Note that the summation in the latter equation starts from $i = 2$, and that the number of differentials in Eqs. (5.16) and (5.21) is the same. A corollary from Eq. (5.21) is the Frumkin equation [29]

$$\left(\frac{\partial \gamma}{\partial \Pi}\right)_{T,\mu_2,\ldots,\mu_k} = h \tag{5.22}$$

For thin liquid films h is a relatively small quantity ($h \leq 10^{-5}$ cm); therefore Eq. (5.22) predicts a rather weak dependence of the film tension γ on the disjoining pressure, Π, in equilibrium thin films. By means of Eqs. (5.3) and (5.15) one can transform Eq. (5.21) to read [28]

$$2d\sigma^f = -\widetilde{s}\,dT - \Pi dh - \sum_{i=2}^{k} \widetilde{\Gamma}_i d\mu_i \tag{5.23}$$

From Eq. (5.23) the following useful relations can be derived [27,28]

$$2\left(\frac{\partial \sigma^f}{\partial h}\right)_{T,\mu_2,\ldots,\mu_k} = -\Pi \qquad \text{(symmetric film)} \tag{5.24}$$

$$\sigma^f(h) = \sigma + \tfrac{1}{2}\int_h^\infty \Pi(h) dh \qquad \text{(symmetric film)} \tag{5.25}$$

Note that the latter two equations differ from the respective relationships for a wetting film,

Eqs (5.7) and (5.8), with multipliers 2 and 1/2; as already mentioned, this is due to the presence of two fluid surfaces in the case of a symmetric liquid film. Note also that the above thermodynamic equations are corollaries from the Gibbs-Duhem equation in the membrane approach, Eq. (5.16).

The *detailed* approach, which treats the two film surfaces as separate surface phases with their own fundamental equations [25,27,30]; thus for a flat symmetric film one postulates

$$dU^f = T dS^f + 2\sigma^f dA + \sum_{i=1}^{k} \mu_i dN_i^f - \Pi A dh, \tag{5.26}$$

where A is area; U^f, S^f and N_i^f are excesses of the internal energy, entropy and number of molecules ascribed to the film surfaces. Compared with the fundamental equation of a simple surface phase [31], Eq. (5.26) contains an additional term, $-\Pi A dh$, which takes into account the dependence of the film surface energy on the film thickness. Equation (5.26) provides an alternative thermodynamic definition of the disjoining pressure:

$$\Pi = -\frac{1}{A}\left(\frac{\partial U^f}{\partial h}\right) \tag{5.27}$$

The thin liquid films formed in foams or emulsions exist in a permanent contact with the bulk liquid in the Plateau borders, encircling the film. From a macroscopic viewpoint, the boundary film / Plateau border can be treated as a three-phase contact line: the line, at which the two surfaces of the Plateau border (the two concave menisci) intersect at the plane of the film, see the right-hand side of Fig. 5.4. The angle α_0, subtended between the two meniscus surfaces, represents the thin film contact angle corresponding to the *membrane* approach. The force balance at each point of the contact line is given by the Neumann-Young equation, Eq. (2.73) with $\sigma_w = \gamma$, and $\sigma_u = \sigma_v = \sigma$. The effect of the line tension, κ, can be also taken into account, see Eq. (2.70). Thus for a symmetrical flat film with circular contact line (Fig. 5.4) one obtains [14]

$$\gamma + \frac{\kappa}{r_0} = 2\sigma \cos\alpha_0 \tag{5.28}$$

where r_0 is the radius of the respective contact line.

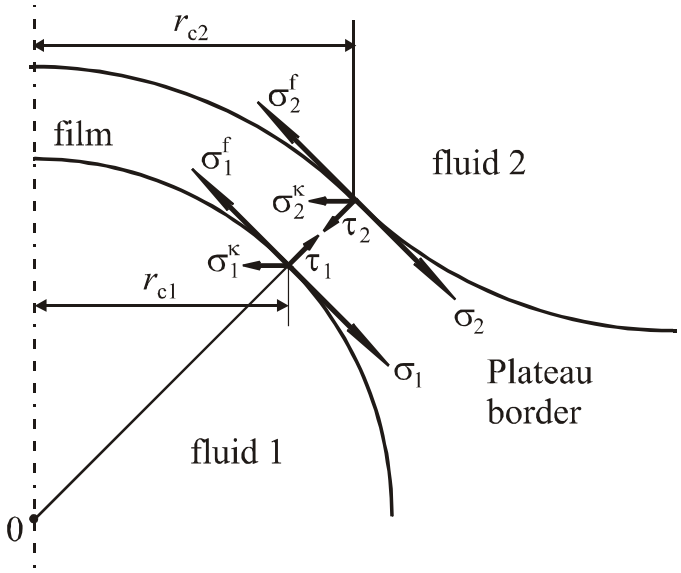

Fig. 5.5. Schematic presentation of the force balances in each point of the two contact lines at the boundary between a spherical film and the Plateau border, see Eq. (5.32); after Refs. [23,32].

There are two film surfaces and two contact lines in the detailed approach, see the left-hand side of Fig. 5.4. They can be treated thermodynamically as linear phases; further, an one-dimensional analogue of Eq. (5.26) can be postulated [14]:

$$dU^L = TdS^L + 2\tilde{\kappa}dL + \sum_i \mu_i dN_i^L + \tau dh \tag{5.29}$$

Here U^L, S^L and N_i^L are linear excesses, $\tilde{\kappa}$ is the line tension in the detailed approach and

$$\tau = \frac{1}{L}\left(\frac{\partial U^L}{\partial h}\right) \tag{5.30}$$

is a thermodynamical definition of the transversal tension, which is apparently an one-dimensional analogue of the disjoining pressure Π – cf. Eqs. (5.27) and (5.30).

The vectorial force balance per unit length of the contact lines of a symmetric film, with account for the line tension effect, is [14]

$$\underline{\boldsymbol{\sigma}} + \underline{\boldsymbol{\sigma}}^f + \underline{\boldsymbol{\tau}} + \underline{\boldsymbol{\sigma}}^\kappa = 0, \qquad |\underline{\boldsymbol{\sigma}}^\kappa| = \tilde{\kappa}/r_c \tag{5.31}$$

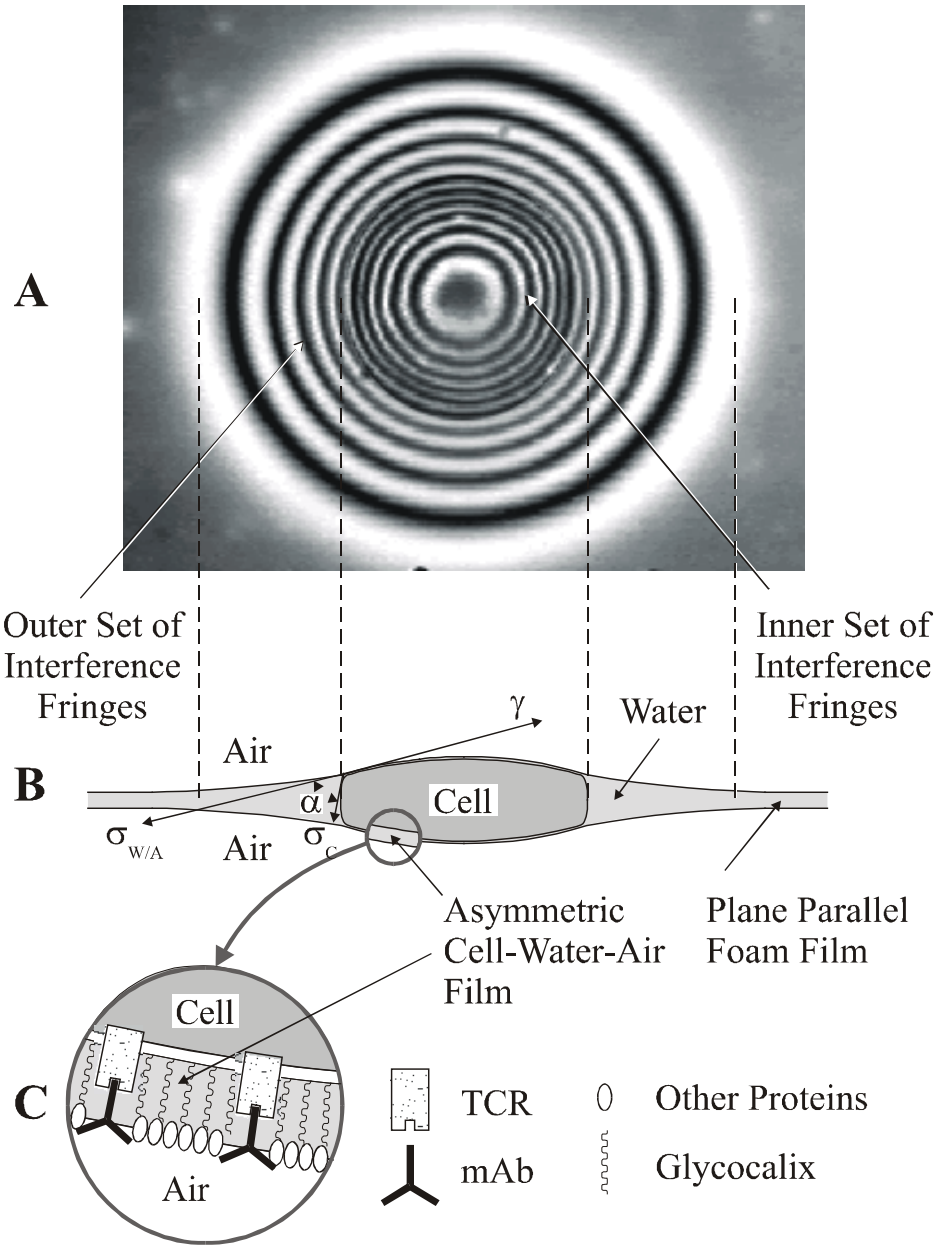

Fig. 5.6. Operation principle of the Film Trapping Technique. (A) A photograph of leukemic Jurkat cell trapped in a foam (air-water-air) film. The cell is observed in reflected monochromatic light; a pattern of alternating dark and bright interference fringes appears. (B) Sketch of the cell trapped in the film. The inner set of fringes corresponds to the region of contact of the cell with the protein adsorption layer (C). From the radii of the interference fringes one can restore the shapes of the liquid meniscus and the cell, and calculate the contact angle, α, the cell membrane tension, σ_C, and the tension of the cell-water-air film, γ; from Ivanov et al. [12]. (TCR = T cell receptor; mAb = monoclonal antibody)

see Fig. 5.4; the vector $\underline{\boldsymbol{\sigma}}^{\kappa}$, expressing the line tension effect, is directed toward the center of curvature of the contact line, see Chapter 2 for details. In the case of a curved or non-symmetric film (film formed between two different fluid phases) Eq. (5.31) can be generalized as follows [23]:

$$\underline{\boldsymbol{\sigma}}_i + \underline{\boldsymbol{\sigma}}_i^f + \underline{\boldsymbol{\tau}}_i + \underline{\boldsymbol{\sigma}}_i^{\kappa} = 0, \qquad i = 1,2 \tag{5.32}$$

see Fig. 5.5 for the notation. Equation (5.32) represents a generalization of the Neumann-Young equation, Eq. (2.73), expressing the vectorial balance of forces at each point of the respective contact line.

Equation (5.32) finds applications for determining contact angles of liquid films, which in their own turn bring information about the interaction energy per unit area of the film, see Eq. 5.10. Experimentally, information about the shape of fluid interfaces can be obtained by means of interferometric techniques and subsequent theoretical analysis of the interference pattern [33]. This approach can be applied also to biological cells. For example, as illustrated in Fig. 5.6, human T cells have been trapped in a liquid film, whose surfaces represent adsorption monolayers of monoclonal antibodies acting as specific ligands for the receptors expressed on the cell surface. From the measured contact angle the cell–monolayer adhesive energy was determined and information about the ligand–receptor interaction has been obtained [12].

5.1.4. DERJAGUIN APPROXIMATION FOR FILMS OF UNEVEN THICKNESS

In the previous sections of this chapter we considered planar liquid films. Here we present a popular approximate approach, proposed by Derjaguin [34], which allows one to calculate the interaction between a particle and an interface across a film of nonuniform thickness, like that depicted in Fig. 5.1b, assuming that the disjoining pressure of a plane-parallel film is known.

Following the derivation by Derjaguin [2, 34], let us consider the zone of contact between a particle and an interface; in general, the latter is curved, see Fig. 5.7a. The "interface" could be the surface of another particle. The Derjaguin approximation is applicable to calculate the interaction between any couple of colloidal particles, either solid, liquid or gas bubbles. The only assumption is that the characteristic range of action of the surface forces is much smaller than any of the surface curvature radii in the zone of contact.

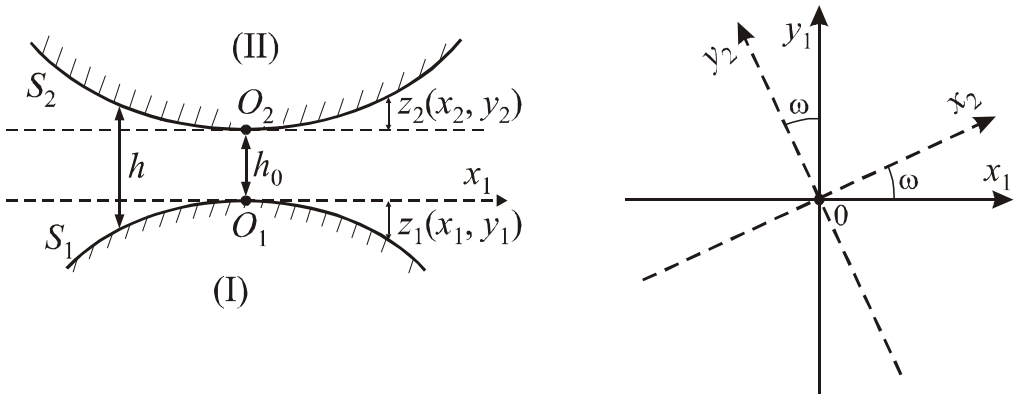

(a) (b)

Fig. 5.7. (a) The zone of contact of two macroscopic bodies; h_0 is the shortest surface-to-surface distance. (b) The directions of the principle curvatures of the two surfaces, in general, subtend some angle ω.

The length of the segment O_1O_2 in Fig. 5.7a, which is the closest distance between the two surfaces, is denoted by h_0. The z-axis is oriented along the segment O_1O_2. In the zone of contact the shapes of the two surfaces can be approximated with paraboloids [2, 34]:

$$z_1 \approx \tfrac{1}{2}c_1x_1^2 + \tfrac{1}{2}c_1'y_1^2, \qquad z_2 \approx \tfrac{1}{2}c_2x_2^2 + \tfrac{1}{2}c_2'y_2^2, \tag{5.33}$$

Here c_1 and c_1' are the principal curvatures of the first surface in the point O_1; likewise, c_2 and c_2' are the principal curvatures of the second surface in the point O_2; the coordinate plane x_iy_i passes through the point O_i, i = 1,2. The axes x_i and y_i are oriented along the principal directions of the curved surface S_i in the point O_i. In general, the directions of the principle curvatures of the two surfaces subtend some angle ω ($0 \le \omega \le 180°$), see Fig. 5.7b:

$$x_2 = x_1\cos\omega + y_1\sin\omega, \qquad y_2 = -x_1\sin\omega + y_1\cos\omega \tag{5.34}$$

The local width of the gap between the two surfaces is (Fig. 5.7a)

$$h = h_0 + z_1 + z_2 \tag{5.35}$$

Combining Eqs. (5.33)–(5.35) one obtains [2, 34]

$$h = h_0 + \tfrac{1}{2}Ax_1^2 + \tfrac{1}{2}By_1^2 + Cx_1y_1 \tag{5.36}$$

where A, B and C are coefficients independent of x_1 and y_1:

$$A = c_1 + c_2 \cos^2\omega + c_2' \sin^2\omega \tag{5.37}$$

$$B = c_1' + c_2 \sin^2\omega + c_2' \cos^2\omega \tag{5.38}$$

$$C = (c_2 - c_2') \cos\omega \sin\omega \tag{5.39}$$

Equation (5.36) expresses $h(x_1, y_1)$ as a bilinear form; the latter, as known from the linear algebra, can be represented as a quadratic form by means of a special coordinate transformation $(x_1, y_1) \rightarrow (x, y)$:

$$h = h_0 + \tfrac{1}{2} c\, x^2 + \tfrac{1}{2} c'\, y^2 \tag{5.40}$$

This is equivalent to bringing of the symmetric matrix (tensor) of the bilinear form into diagonal form:

$$\begin{pmatrix} \frac{1}{2}A & \frac{1}{2}C \\ \frac{1}{2}C & \frac{1}{2}B \end{pmatrix} \rightarrow \begin{pmatrix} \frac{1}{2}c & 0 \\ 0 & \frac{1}{2}c' \end{pmatrix} \tag{5.41}$$

Since the determinant of a tensor is invariant with respect to coordinate transformations, one can write

$$c\,c' = AB - C^2 \tag{5.42}$$

Further, we assume that the interaction free energy (due to the surface forces) per unit area of a plane-parallel film of thickness h is known: this is the function $f(h)$ defined by Eq. (5.9). The "core" of the Derjaguin approximation is the assumption that the energy of interaction, U, between the two bodies (I and II in Fig. 5.7a) across the film is given by the expression

$$U = \iint f(h(x, y))\, dxdy \tag{5.43}$$

where $h = h_0 + \tfrac{1}{2} c\, x^2 + \tfrac{1}{2} c'\, y^2$. Further, let us introduce polar coordinates in the plane xy:

$$x = \frac{\rho}{\sqrt{c}} \cos\varphi\,, \qquad y = \frac{\rho}{\sqrt{c'}} \cos\varphi \tag{5.44}$$

Since h depends only on ρ, Eq. (4.43) acquires the form

$$U = \int_0^{2\pi} \int_0^{\infty} f(h(\rho)) \frac{\rho d\rho d\varphi}{\sqrt{cc'}} \qquad (h = h_0 + \tfrac{1}{2}\rho^2) \tag{5.45}$$

Integrating with respect to φ and using the relationship $dh = \rho d\rho$ one finally obtains [2, 34]

$$U(h_0) = \frac{2\pi}{\sqrt{E}} \int_{h_0}^{\infty} f(h) dh, \qquad \text{(interaction energy)} \tag{5.46}$$

$$E \equiv cc' = c_1 c_1' + c_2 c_2' + (c_1 c_2 + c_1' c_2') \sin^2 \omega \; + (c_1 c_2' + c_1' c_2) \cos^2 \omega \tag{5.47}$$

The last expression is obtained by substitution of Eqs (5.37)–(5.39) into Eq. (5.42). We recall that ω is the angle subtended between the directions of the principle curvatures of the two approaching surfaces. It has been established, both experimentally [3] and theoretically [35], that Eq. (5.46) provides a good approximation for the interaction energy in the range of its validity. The interaction force between two bodies, separated at a surface-to-surface distance h_0, can be obtained by differentiation of Eq. (5.46):

$$F(h_0) = -\frac{\partial U}{\partial h_0} = \frac{2\pi}{\sqrt{E}} f(h_0) \qquad \text{(interaction force)} \tag{5.48}$$

Next, we consider various cases of special geometry:

Sphere–Wall: This is the configuration depicted in Fig. 5.1b – particle of radius R situated at a surface-to-surface distance h_0 from a planar solid surface. In such a case $c_1 = c_1' = 1/R$, whereas $c_2 = c_2' = 0$. Then from Eqs. (5.46)–(5.47) one deduces

$$U(h_0) = 2\pi R \int_{h_0}^{\infty} f(h) dh, \qquad \text{(sphere–wall)} \tag{5.49}$$

Truncated Sphere – Wall: For this configuration, see Fig. 5.1a, the interaction across the plane-parallel film of radius r_c should be also taken into account [36-39]:

$$U(h_0) = 2\pi R \int_{h_0}^{\infty} f(h) dh + \pi r_c^2 f(h_0) \qquad \text{(truncated sphere – wall)} \tag{5.50}$$

Two Spheres: For two spherical particles of radii R_1 and R_2 separated at a surface-to-surface distance h_0 one has $c_1 = c_1' = 1/R_1$ and $c_2 = c_2' = 1/R_2$. Then Eqs. (5.46)–(5.47) yield

$$U(h_0) = \frac{2\pi R_1 R_2}{R_1 + R_2} \int_{h_0}^{\infty} f(h)\, dh \qquad \text{(two spheres)} \qquad (5.51)$$

In the limit $R_1 \to R$ and $R_2 \to \infty$ Eq. (5.51) reduces to Eq. (5.49), as it should be expected.

Two Crossed Cylinders: For two infinitely long cylinders (rods) of radii r_1 and r_2, which are separated at a transversal surface-to-surface distance h_0, and whose axes subtend an angle ω, one has $c_1 = 1/r_1$, $c_1' = 0$, $c_2 = 1/r_2$ and $c_2' = 0$. Then Eqs. (5.46)–(5.47) lead to [2]

$$U(h_0) = \frac{2\pi\sqrt{r_1 r_2}}{\sin\omega} \int_{h_0}^{\infty} f(h)\, dh \qquad \text{(two cylinders)} \qquad (5.52)$$

The latter equation is often used to interpret data obtained by means of the surface force apparatus, which operates with crossed cylinders [3]. For parallel cylinders, that is for $\omega \to 0$, Eq. (5.52) gives $U \to \infty$; this divergence is not surprising because the contact zone between two parallel cylinders is infinitely long, whereas the interaction energy per unit length is finite. In the surface force apparatus usually $\omega = 90°$ and then $\sin\omega = 1$.

The interaction force can be calculated by a mere differentiation of Eqs. (5.49)–(5.52) in accordance with Eq. (5.48).

The Derjaguin approximation is applicable to any type of force law (attractive, repulsive, oscillatory) if only the range of the forces is much smaller than the particle radii. Moreover, it is applicable to any kind of surface force, irrespective of its physical origin: van der Waals, electrostatic, steric, oscillatory-structural, etc. forces, which are described in the next section.

5.2. INTERACTIONS IN THIN LIQUID FILMS

5.2.1. OVERVIEW OF THE TYPES OF SURFACE FORCES

As already mentioned, if a liquid film is sufficiently thin (thinner than c.a. 100 nm) the interaction of the two neighboring phases across the film is not negligible. The resulting disjoining pressure, $\Pi(h)$, may contain contributions from various kinds of molecular interactions.

The first successful theoretical model of the interactions in liquid films and the stability of

colloidal dispersions was created by Derjaguin & Landau [16], and Verwey & Overbeek [17]; it is often termed "DLVO theory" after the names of the authors. This model assumes that the disjoining pressure is a superposition of *electrostatic repulsion* and *van der Waals attraction*, see Eq. (5.12), Fig. 5.3 and Sections 5.2.2 and 5.2.4 below. In many cases this is the correct physical picture and the DLVO theory provides a quantitative description of the respective effects and phenomena.

Subsequent studies, both experimental and theoretical, revealed the existence of other surface forces, different from the conventional van der Waals and electrostatic (double layer) interactions. Such forces appear as deviations from the DLVO theory and are sometimes called "non-DLVO surface forces" [3]. An example is the *hydrophobic attraction* which brings about instability of aqueous films spread on a hydrophobic surface, see Section 5.2.3. Another example is the *hydration repulsion*, which appears as a considerable deviation from the DLVO theory in very thin ($h < 10$ nm) films from electrolyte solutions, see Section 5.2.5.

Oscillations of the surface force with the surface-to-surface distance were first detected in films from electrolyte solutions sandwiched between solid surfaces [3, 40]. This *oscillatory structural force* appears also in thin liquid films containing small colloidal particles like surfactant micelles, polymer coils, protein macromolecules, latex or silica particles [41]. For larger particle volume fractions the oscillatory force is found to stabilize thin films and dispersions, whereas at low particle concentrations it degenerates into the *depletion attraction*, which has the opposite effect, see Section 5.2.7.

When the surfaces of the liquid film are covered with adsorption layers form nonionic surfactants, like those having polyoxiethylene moieties, the overlap of the formed polymer brushes give rise to a *steric interaction* [3, 42], which is reviewed in Section 5.2.8.

The surfactant adsorption monolayers on liquid interfaces and the lipid lamellar membranes are involved in a thermally exited motion, which manifests itself as fluctuation capillary waves. When such two interfaces approach each other, the overlap of the interfacial corrugations causes a kind of steric interaction (though a short range one), termed the *fluctuation force* [3], see Section 5.2.9.

The approach of a fluid particle (emulsion drop or gas bubble) to a phase boundary might be

accompanied with interfacial deformations: dilatation and bending. The latter also do contribute to the overall particle–surface interaction, see Section 5.2.10. In a final reckoning, the total energy of interaction between a particle and a surface, U, can be expressed as a sum of contributions of different origin: from the interfacial dilatation and bending, from the van der Waals, electrostatic, hydration, oscillatory-structural, steric, etc. surface forces as follows [43]:

$$U = U_{\text{dil}} + U_{\text{bend}} + U_{\text{vw}} + U_{\text{el}} + U_{\text{hydr}} + U_{\text{osc}} + U_{\text{st}} + \cdots \tag{5.53}$$

Below we present theoretical expressions for calculating the various terms in the right-hand side of Eq. (5.53). In addition, in the next Chapter 6 we consider also the surface forces of *hydrodynamic* origin, which are due to the viscous dissipation of energy in the narrow gap between two approaching surfaces in liquid (Section 6.2).

In summary, below in this chapter we present a brief description of the various kinds of surface forces. The reader could find more details in the specialized literature on surface forces and thin liquid films [2, 3, 42-45]

5.2.2. VAN DER WAALS SURFACE FORCE

The van der Waals forces represent an averaged dipole-dipole interaction, which is a superposition of three contributions: (i) *orientation interaction* between two permanent dipoles: effect of Keesom [46]; (ii) *induction interaction* between one permanent dipole and one induced dipole: effect of Debye [47]; (iii) *dispersion interaction* between two induced dipoles: effect of London [48]. The energy of van der Waals interaction between molecules i and j obeys the law [49]

$$u_{ij}(r) = -\frac{\alpha_{ij}}{r^6} \tag{5.54}$$

where u_{ij} is the potential energy of interaction, r is the distance between the two molecules and α_{ij} is a constant characterizing the interaction. In the case of two molecules in a gas phase one has [3, 49]

$$\alpha_{ij} = \frac{p_i^2 p_j^2}{3kT} + \left(p_i^2 \alpha_{0j} + p_j^2 \alpha_{0i}\right) + \frac{3\pi \alpha_{0i} \alpha_{0j} h_P \nu_i \nu_j}{\nu_i + \nu_j} \tag{5.55}$$

where p_i and α_{0i} are molecular dipole moment and electronic polarizability, $h_P = 6.63\times10^{-34}$ J.s is the Planck constant and ν_i can be interpreted as the orbiting frequency of the electron in the Bohr atom; see Refs. [3, 50] for details.

The van der Waals interaction between two macroscopic bodies can be found by integration of Eq. (5.54) over all couples of interacting molecules followed by subtraction of the interaction energy at infinite separation between the bodies. The result of integration depends on the geometry of the system. For a *plane-parallel film* located between two semiinfinite phases the van der Waals interaction energy per unit area and the respective disjoining pressure, stemming from Eq. (5.54), are [51]:

$$f_{\rm vw} = -\frac{A_{\rm H}}{12\pi h^2}, \qquad \Pi_{\rm vw} = -\frac{\partial f_{\rm vw}}{\partial h} = -\frac{A_{\rm H}}{6\pi h^3} \tag{5.56}$$

where, as usual, h is the thickness of the film and $A_{\rm H}$ is the Hamaker constant [44, 51]; about the calculation of $A_{\rm H}$ – see Eqs. (5.65)–(5.74) below. By integration over all couples of interacting molecules Hamaker [51] has derived the following expression for the energy of van der Waals interaction between *two spheres* of radii R_1 and R_2:

$$U_{\rm vw}(h_0) = -\frac{A_H}{12}\left(\frac{y}{x^2+xy+x} + \frac{y}{x^2+xy+x+y} + 2\ln\frac{x^2+xy+x}{x^2+xy+x+y}\right) \tag{5.57}$$

where

$$x = h_0 / 2R_1, \qquad y = R_2 / R_1 \le 1 \tag{5.58}$$

as before, h_0 is the shortest surface-to-surface distance. For $x << 1$ Eq. (5.57) reduces to

$$U_{\rm vw}(h_0) \approx -\frac{A_{\rm H}}{12}\frac{y}{(1+y)x} = -\frac{2\pi R_1 R_2}{R_1+R_2}\frac{A_{\rm H}}{12\pi h_0} \tag{5.59}$$

Equation (5.59) can be also derived by substituting $f_{\rm vw}(h)$ from Eq. (5.56) into Derjaguin approximation (5.51). It is worthwhile noting, that the logarithmic term in Eq. (5.57) can be neglected only if $x << 1$. For example, even when $x = 5\times10^{-3}$, the contribution of the

logarithmic term amounts to about 10% of the result (for $y = 1$); consequently, for larger values of x this term must be retained [44].

For the configuration *sphere – wall*, which is depicted in Fig. 5.1b, an expression for the interaction energy can be obtained setting $R_1 \to \infty$ and $R_2 = R$ in Eqs. (5.57) and (5.58):

$$U_{\mathrm{vw}}(h_0) = -\frac{A_H}{12}\left(\frac{2R}{h_0} + \frac{2R}{2R+h_0} + 2\ln\frac{h_0}{2R+h_0}\right) \tag{5.60}$$

Alternatively, substituting $f_{\mathrm{vw}}(h)$ from Eq. (5.56) into the Derjaguin approximated formula (5.49) one derives

$$U_{\mathrm{vw}}(h_0) \approx -\frac{A_H}{12}\frac{2R}{h_0} \tag{5.61}$$

which coincides with the leading term in Eq. (5.60) for $h_0/(2R) << 1$.

Next, let us consider the configuration *truncated sphere – wall*, which is depicted in Fig. 5.1a. An expression for the interaction energy in this case has been derived by Danov et al. [37]:

$$U_{\mathrm{vw}}(h_0) = -\frac{A_H}{12}\left(\frac{2R}{h_0} + \frac{r_c^2}{h_0^2} + \frac{2R}{l+h_0} + 2\ln\frac{h_0}{l+h_0} - \frac{2r_c^2}{lh}\right) \tag{5.62}$$

where $l \equiv R + (R^2 - r_c^2)^{1/2}$. Alternatively, substituting $f_{\mathrm{vw}}(h)$ from Eq. (5.56) into Derjaguin approximated formula (5.50) one obtains

$$U_{\mathrm{vw}}(h_0) \approx -\frac{A_H}{12}\left(\frac{2R}{h_0} + \frac{r_c^2}{h_0^2}\right) \tag{5.63}$$

Obviously, the latter approximate expression contains the two leading terms in the right-hand side of Eq. (5.62) for $h_0 \to 0$.

In the case of film between *two identical deformed emulsion droplets*, like those depicted in Fig. 3.5 with $a = R$, $r = r_c$ and $h = h_0$, the respective droplet-droplet interaction energy can be expressed in the form [37]

$$U_{\mathrm{vw}}(h_0) \approx -\frac{A_H}{12}\left[\frac{R}{h_0} + \frac{r_c^2}{h_0^2} + \frac{3}{4} + 2\ln\left(\frac{h_0}{R}\right) - \frac{2r_c^2}{Rh_0}\right] \qquad (h_0, r_c << R) \tag{5.64}$$

Equation (5.64) represents a truncated series expansion; the *exact formula*, which is rather long, can be found in Ref. [37]. Expressions for U_{vw} for other geometrical configurations are also available [52].

Further, we consider expressions for calculating the Hamaker constant A_H, which enters Eqs. (5.56)–(5.64). For that purpose two approaches have been developed: the *microscopic* theory due to Hamaker [51] and the *macroscopic* theory due to Lifshitz [53].

Microscopic theory: its basic assumption is that the van der Waals interaction is pair-wise additive, and consequently, the total interaction energy between two bodies can be obtained by interaction over all couples of constituent molecules. Thus, for the interaction between two semiinfinite phases, composed from components *i* and *j*, across a plane-parallel gap of *vacuum*, one obtains Eq. (5.56) with $A_H = A_{ij}$, where A_{ij} is expressed as follows

$$A_{ij} = \pi^2 \rho_i \rho_j \alpha_{ij} \tag{5.65}$$

ρ_i and ρ_j are the densities of the respective phases and α_{ij} is a molecular parameter defined by Eq. (5.55). Usually, the dimension of ρ_i and ρ_j is expressed in molecules per cm^3, and then A_H and A_{ij} have a dimension of energy.

For a plane-parallel film from component 3 between two semiinfinite phases from components 1 and 2 the microscopic approach gives again Eq. (5.56), but this time the compound Hamaker constant is determined by the expression [44]

$$A_H \equiv A_{132} = A_{33} + A_{12} - A_{13} - A_{23} \tag{5.66}$$

Here A_{ij} (i,j = 1,2,3) is determined by Eq. (5.65). If the film is "filled" with vacuum, then $\rho_3 = 0$ and Eq. (5.66) reduces to $A_H = A_{12}$, as it could be expected. If the Hamaker constants of the symmetric films, viz. A_{ii} and A_{jj}, are known, one can estimate A_{ij} ($i \neq j$) by using the approximation of Hamaker

$$A_{ij} = \left(A_{ii} A_{jj}\right)^{1/2} \tag{5.67}$$

If components 1 and 2 are identical, A_H is positive. Therefore, the van der Waals interaction between identical bodies is *attractive* across any medium. Besides, two dense bodies (even if nonidentical) will attract each other when placed in medium 3 of low density (gas, vacuum).

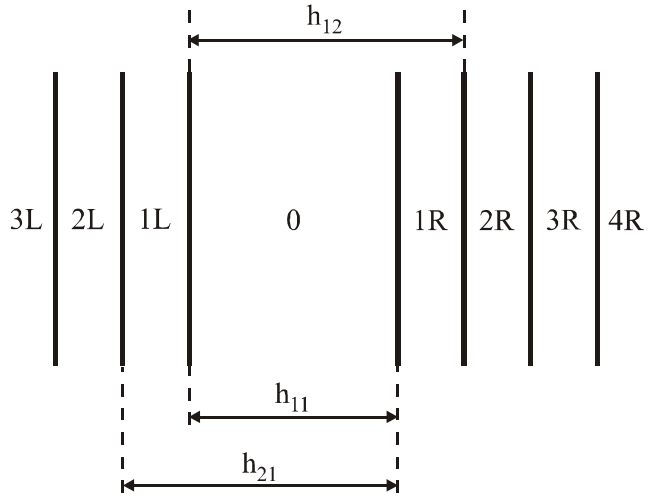

Fig. 5.8. Sketch of two multilayered bodies interacting across a medium 0; the layers are counted from the central film 0 outward to the left (L) and right (R).

On the other hand, if the phase in the middle (component 3) has an intermediate Hamaker constant between those of bodies 1 and 2 (say $A_{11} < A_{33} < A_{22}$), then the compound Hamaker constant A_H can be negative and the van der Waals disjoining pressure can be *repulsive* (positive). Such is the case of an aqueous film between mercury and gas [54], or liquid hydrocarbon film on alumina [55] and quartz [56]. It is worthwhile noting that the liquid helium climbs up the walls of containers because of the repulsive van der Waals force across the wetting helium film [3, 57, 58].

Equation (5.66) can be generalized for multilayered films. For example, two surfactant adsorption monolayers (or lipid bilayers) interacting across water film can be modeled as a multilayered structure: one layer for the headgroup region, other layer for the hydrocarbon tails, another layer for the aqueous core of the film, etc.). There is a general formula for the interaction between two such multilayered structures (Fig. 5.8) stemming from the microscopic approach [52]:

$$f_{\mathrm{vw}} = -\sum_{i=1}^{N_L}\sum_{j=1}^{N_R} \frac{A(i,j)}{12\pi h_{ij}^2}, \qquad A(i,j) \equiv A_{i,j} - A_{i,j-1} - A_{i-1,j} + A_{i-1,j-1} \tag{5.68}$$

where N_{L} and N_{R} denote the number of layers on the *left* and on the *right* from the central layer, the latter denoted by index "0" – see Fig. 5.8 for the notation; $A_{i,j}$ (= A_{ij}) is defined by Eq. (5.65). Equation (5.68) reduces to Eq. (5.56) for $N_{\mathrm{L}} = N_{\mathrm{R}} = 1$ and $h_{11} = h$.

Macroscopic theory: An alternative approach to the calculation of the Hamaker constant A_H in condensed phases is provided by the Lifshitz theory [53, 57], which is not limited by the assumption for pairwise additivity of the van der Waals interaction, see also Refs. [2, 3, 52]. The Lifshitz theory treats each phase as a continuous medium characterized by a given uniform dielectric permittivity, which is dependent on the frequency, ν, of the propagating electromagnetic waves. A good knowledge of quantum field theory is required to understand the Lifshitz theory of the van der Waals interaction between macroscopic bodies. Nevertheless, the final results of this theory can be represented in a form convenient for application. For the symmetric configuration of two identical phases i interacting across a medium j the macroscopic theory provides the expression [3]

$$A_H \equiv A_{iji} = A_{iji}^{(\nu=0)} + A_{iji}^{(\nu>0)} = \frac{3}{4}kT\left(\frac{\varepsilon_i - \varepsilon_j}{\varepsilon_i + \varepsilon_j}\right)^2 + \frac{3h_P\nu_e\left(n_i^2 - n_j^2\right)^2}{16\sqrt{2}\left(n_i^2 + n_j^2\right)^{3/2}} \tag{5.69}$$

where ε_i and ε_j are the dielectric constants of phases i and j; n_i and n_j are the respective refractive indices for visible light; as usual, h_P is the Planck constant; ν_e is the main electronic absorption frequency which is $\approx 3.0\times10^{15}$ Hz for water and the most organic liquids [3]. The first term in the right-hand side of Eq. (5.69), $A_{iji}^{(\nu=0)}$, the so called *zero frequency term*, expresses the contribution of the orientation and induction interactions. Indeed, these two contributions to the van der Waals force represent electrostatic effects. Equation (5.69) shows that this zero-frequency term can never exceed $\frac{3}{4}kT \approx 3\times10^{-21}$ J. The last term in Eq. (5.69), $A_{iji}^{(\nu>0)}$, accounts for the *dispersion* interaction. If the two phases, i and j, have comparable densities (as it is for emulsion systems, say oil–water–oil), then $A_{iji}^{(\nu>0)}$ and $A_{iji}^{(\nu=0)}$ are comparable by magnitude. If one of the phases, i or j, has low density (gas, vacuum), as a rule $A_{iji}^{(\nu>0)} >> A_{iji}^{(\nu=0)}$; in this respect the macroscopic and microscopic theories often give different predictions for the value of A_{H}.

For the more general configuration of phases i and k, interacting across a film from phase j, the macroscopic (Lifshitz) theory provides the following expression [3]

$$A_H \equiv A_{ijk} \equiv A_{ijk}^{(\nu=0)} + A_{ijk}^{(\nu>0)} = \frac{3}{4}kT\left(\frac{\varepsilon_i - \varepsilon_j}{\varepsilon_i + \varepsilon_j}\right)\left(\frac{\varepsilon_k - \varepsilon_j}{\varepsilon_k + \varepsilon_j}\right) + \frac{3h_P\nu_e\left(n_i^2 - n_j^2\right)\left(n_k^2 - n_j^2\right)}{8\sqrt{2}\left(n_i^2 + n_j^2\right)^{1/2}\left(n_k^2 + n_j^2\right)^{1/2}\left[\left(n_i^2 + n_j^2\right)^{1/2} + \left(n_k^2 + n_j^2\right)^{1/2}\right]} \tag{5.70}$$

Upon substitution $k = i$ Eq. (5.70) reduces to Eq. (5.69). Equation (5.70) can be simplified if the following approximate relationship is satisfied:

$$\frac{1}{2}\left[\left(n_i^2 + n_j^2\right)^{1/2} + \left(n_k^2 + n_j^2\right)^{1/2}\right] \approx \left[\left(n_i^2 + n_j^2\right)^{1/2}\left(n_k^2 + n_j^2\right)^{1/2}\right]^{1/2}, \tag{5.71}$$

that is the arithmetic and geometric mean of the respective quantities are approximately equal. Substitution of Eq. (5.71) into (5.70) yields a more compact expression:

$$A_H \equiv A_{ijk} \approx \frac{3}{4}kT\left(\frac{\varepsilon_i - \varepsilon_j}{\varepsilon_i + \varepsilon_j}\right)\left(\frac{\varepsilon_k - \varepsilon_j}{\varepsilon_k + \varepsilon_j}\right) + \frac{3h_P\nu_e\left(n_i^2 - n_j^2\right)\left(n_k^2 - n_j^2\right)}{16\sqrt{2}\left(n_i^2 + n_j^2\right)^{3/4}\left(n_k^2 + n_j^2\right)^{3/4}} \tag{5.72}$$

Comparing Eqs. (5.69) and (5.72) one obtains the following *combining relations*:

$$A_{ijk}^{(\nu=0)} = \left[A_{iji}^{(\nu=0)} A_{kjk}^{(\nu=0)}\right]^{1/2} \tag{5.73}$$

$$A_{ijk}^{(\nu>0)} \approx \left[A_{iji}^{(\nu>0)} A_{kjk}^{(\nu>0)}\right]^{1/2} \tag{5.74}$$

The latter two equations show that according to the macroscopic theory the Hamaker approximation, Eq. (5.67), holds separately for the zero-frequency term, $A_{ijk}^{(\nu=0)}$ (orientation + induction interactions) and for the dispersion interaction term, $A_{ijk}^{(\nu>0)}$.

Effect of electromagnetic retardation. The asymptotic behavior of the *dispersion* interaction at large intermolecular separations does not obey Eq. (5.54); instead $u_{ij} \propto 1/r^7$ due to the electromagnetic retardation effect established by Casimir and Polder [59]. Experimentally this effect has been first detected by Derjaguin and Abrikossova [60] in measurements of the interaction between two quartz glass surfaces in the distance range 100–400 nm. Various expressions have been proposed to account for this effect in the Hamaker constant; one convenient formula for the case of symmetric films has been derived by Prieve and Russel, see

Ref. [42]:

$$A_{iji}^{(\nu>0)} = \frac{3h_P\nu_e}{4\pi}\frac{\left(n_i^2-n_j^2\right)^2}{\left(n_i^2+n_j^2\right)^{3/2}}\int_0^\infty \frac{\left(1+2\tilde{h}z\right)\exp\left(-2\tilde{h}z\right)}{\left(1+2z^2\right)^2}dz \tag{5.75}$$

where, as usual, h is the film thickness; the dimensionless thickness $\tilde{h}$ is defined by the expression

$$\tilde{h} = n_j\left(n_i^2+n_j^2\right)^{1/2}\frac{2\pi\nu_e h}{c}\ , \tag{5.76}$$

where $c = 3.0 \times 10^{10}$ cm/s is the speed of light; the integral in Eq. (5.75) is to be solved numerically; for estimates one can use the approximate interpolating formula [42]:

$$\int_0^\infty \frac{\left(1+2\tilde{h}z\right)\exp\left(-2\tilde{h}z\right)}{\left(1+2z^2\right)^2}dz \approx \frac{\pi}{4\sqrt{2}}\left[1+\left(\frac{\pi\tilde{h}}{4\sqrt{2}}\right)^{3/2}\right]^{-2/3} \tag{5.77}$$

For small thickness $A_{iji}^{(\nu>0)}$, as given by Eqs. (5.75), is constant, whereas for large thickness h one obtains $A_{iji}^{(\nu>0)} \propto h^{-1}$. For additional information about the electromagnetic retardation effect – see Refs. [3, 42, 52]. It is interesting to note that this relativistic effect essentially influences the critical thickness of rupture of foam and emulsion films, see Section 6.2 below.

Screening of the orientation and induction interactions in electrolyte solutions. As already mentioned, the orientation and induction interactions (unlike the dispersion interaction) are electrostatic effects; so, they are not subjected to electromagnetic retardation. Instead, they are influenced by the Debye screening due to the presence of ions in the aqueous phase. Thus for the interaction across an electrolyte solution the screened Hamaker constant is given by the expression [50]

$$A_H = A^{(\nu=0)}(2\kappa h)e^{-2\kappa h} + A^{(\nu>0)} \tag{5.78}$$

where $A^{(\nu=0)}$ denotes the contribution of orientation and induction interaction into the Hamaker constant in the absence of any electrolyte; $A^{(\nu>0)}$ is the contribution of the dispersion interaction; κ is the Debye screening parameter defined by Eqs. (1.56) and (1.64). Additional information about this effect can be found in Refs. [3, 42, 50].

5.2.3. LONG-RANGE HYDROPHOBIC SURFACE FORCE

The experiment sometimes gives values of the Hamaker constant, which are markedly larger than the values predicted by the theory. This fact could be attributed to the action of a strong attractive *hydrophobic force*, which is found to appear across thin aqueous films sandwiched between two hydrophobic surfaces [61-63]. The experiments showed that the nature of the hydrophobic force is different from the van der Waals interaction [61-69]. It turns out that the hydrophobic interaction decays exponentially with the increase of the film thickness, h. The hydrophobic free energy per unit area of the film can be described by means of the equation [3]

$$f_{\text{hydrophobic}} = -2\gamma e^{-h/\lambda_0} \tag{5.79}$$

where typically γ = 10-50 mJ/m^2, and λ_0 = 1-2 nm in the range $0 < h < 10$ nm. Larger decay length, λ_0 = 12-16 nm, was reported by Christenson *et al.* [69] for the range 20 nm $< h <$ 90 nm. This long-ranged attraction entirely dominates over the van der Waals forces. The fact that the hydrophobic attraction can exist at high electrolyte concentrations, of the order of 1 M, means that this force cannot have electrostatic origin [69-74]. In practice, this attractive interaction leads to a rapid coagulation of hydrophobic particles in water [75, 76] and to rupturing of water films spread on hydrophobic surfaces [77]. It can play a role in the adhesion and fusion of lipid bilayers and biomembranes [78]. The hydrophobic interaction can be completely suppressed if the adsorption of surfactant, dissolved in the aqueous phase, converts the surfaces from hydrophobic into hydrophilic.

There is no generally accepted explanation of the hydrophobic force [79]. One of the possible mechanisms is that an orientational ordering, propagated by hydrogen bounds in water and other associated liquids, could be the main underlying factor [3, 80]. Another hypothesis for the physical origin of the hydrophobic force considers a possible role of formation of gaseous capillary bridges between the two hydrophobic surfaces [65, 3, 72], see Fig. 2.6a. In this case the hydrophobic force would be a kind of capillary-bridge force; see Chapter 11 below. Such bridges could appear spontaneously, by nucleation (spontaneous dewetting), when the distance between the two surfaces becomes smaller than a certain threshold value, of the order of several hundred nanometers, see Table 11.2 below. Gaseous bridges could appear even if there is no dissolved gas in the water phase; the pressure inside a bridge can be as low as the equilibrium

vapor pressure of water (23.8 mm Hg at 25°C) owing to the high interfacial curvature of nodoid-shaped bridges, see Chapter 11. A number of recent studies [81-88] provide evidence in support of the capillary-bridge origin of the long-range hydrophobic surface force. In particular, the observation of "steps" in the experimental data was interpreted as an indication for separate acts of bridge nucleation [87].

5.2.4. ELECTROSTATIC SURFACE FORCE

The electrostatic (double layer) interactions across an aqueous film are due to the overlap of the double electric layers formed at two charged interfaces. The surface charge can be due to dissociation of surface ionizable groups or to the adsorption of ionic surfactants (Fig. 1.4) and polyelectrolytes [2,3]. Note however, that sometimes electrostatic repulsion is observed even between interfaces covered by adsorption monolayers of nonionic surfactants [89-92].

First, let us consider the electrostatic (double layer) interaction between two *identical* charged plane parallel surfaces across a solution of an electrolyte (Fig. 5.9). If the separation between the two planes is very large, the number concentration of both counterions and coions would be equal to its bulk value, n_0, in the middle of the film. However, at finite separation, h, between the surfaces the two electric double layers overlap and the counterion and coion concentrations in the middle of the film, n_{1m} and n_{2m}, are not equal. As pointed out by Langmuir [93], the *electrostatic* disjoining pressure, Π_{el}, can be identified with the excess osmotic pressure in the middle of the film:

$$\Pi_{el} = kT\left(n_{1m} + n_{2m} - 2n_0\right) \tag{5.80}$$

One can deduce Eq. (5.80) starting from a more general definition of disjoining pressure [2, 23]:

$$\Pi = P_N - P_{bulk} \tag{5.81}$$

where P_N is the normal (with respect to the film surface) component of the pressure tensor $\mathbf{P}$ and P_{bulk} is the pressure in the bulk of the electrolyte solution. The condition for mechanical equilibrium, $\nabla\cdot\mathbf{P} = 0$, yields $\partial P_N/\partial z = 0$, that is P_N = const. across the film; the z-axis is directed

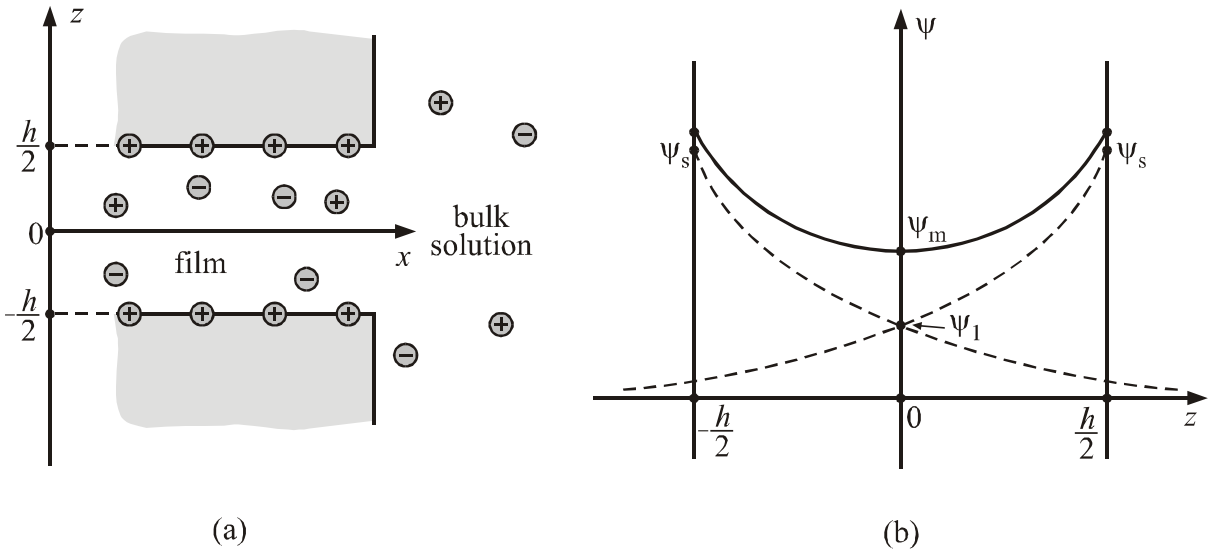

Fig. 5.9. (a) Schematic presentation of a liquid film from electrolyte solution between two identical charged surfaces; the film is equilibrated with the bulk solution. (b) Distribution $\psi(z)$ of the electric potential across the liquid film (the continuous line): ψ_m is the minimum value of $\psi(z)$ in the middle of the film; the dashed lines show the electric potential distribution created by the respective charged surfaces in contact with a semiinfinite electrolyte solution.

perpendicular to the film surfaces, Fig. 5.9a. Hence Π, defined by Eq. (5.81), has a constant value for a given liquid film at a given thickness.

For a liquid film from electrolyte solution one can use Eq. (1.17) to express P_N :

$$P_N \equiv P_{zz} = P_o(z) - \frac{\varepsilon}{8\pi}\left(\frac{d\psi}{dz}\right)^2 \tag{5.82}$$

where, as usual, $\psi(z)$ is the potential of the electric field, ε is the dielectric permittivity of the solution, $P_o(z)$ is the pressure in a uniform phase, which is in chemical equilibrium with the bulk electrolyte solution and has the same composition as the film at level z. Considering the electrolyte solution as an ideal solution, and using the known expression for the osmotic pressure, we obtain

$$P_o(z) - P_{bulk} = kT[n_1(z) + n_2(z) - 2n_0] \tag{5.83}$$

where $n_1(z)$ and $n_2(z)$ are local concentrations of the counterions and coions inside the film. The combination of Eqs. (5.81)–(5.83) yields

$$\Pi_{el} = kT\,[n_1(z) + n_2(z) - 2n_0] - \frac{\varepsilon}{8\pi}\left(\frac{d\psi}{dz}\right)^2 \tag{5.84}$$

Equation (5.84) represents a general definition for the electrostatic component of disjoining pressure, which is valid for symmetric and non-symmetric electrolytes, as well as for identical and nonidentical film surfaces. The same equation was derived by Derjaguin [44] in a different, thermodynamic manner.

Note that Π_{el}, defined by Eq. (5.84), must be constant, i.e. independent of the coordinate z. To check that one can use the equations of Boltzmann and Poisson:

$$n_i(z) = n_0 \exp[-Z_i e\psi(z)/kT] \tag{5.85}$$

$$\frac{d^2\psi}{dz^2} = -\frac{4\pi}{\varepsilon}\sum_i Z_i e n_i(z) \tag{5.86}$$

Let us multiply Eq. (5.86) with $d\psi/dz$, substitute $n_i(z)$ from Eq. (5.85) and integrate with respect to z; the result can be presented in the form

$$\frac{\varepsilon}{8\pi}\left(\frac{d\psi}{dz}\right)^2 - kT\sum_i n_i(z) = \text{const.} \tag{5.87}$$

The latter equation, along with Eq. (5.84), proves the constancy of Π_{el} across the film.

If the film has identical surfaces, the electric potential has an extremum in the midplane of the film, $(d\psi/dz)_{z=0} = 0$, see Fig. 5.9b. Then from Eq. (5.87) one obtains

$$\frac{\varepsilon}{8\pi}\left(\frac{d\psi}{dz}\right)^2 - kT\,[n_1(z) + n_2(z)] = -kT\,(n_{1m} + n_{2m}) \tag{5.88}$$

where $n_{im} \equiv n_i(0)$, $i = 1,2$. One can check that the substitution of Eq. (5.88) into Eq. (5.84) yields the Langmuir expression for Π_{el}, that is Eq. (5.80).

To obtain the dependence of Π_{el} on the film thickness h, one has to first determine the dependence of n_{1m} and n_{2m} on h by solving the Poisson-Boltzmann equation, and then to substitute the result in the definition (5.80). This was done rigorously by Derjaguin and Landau [16], who obtained an equation in terms of elliptic integrals, see also Refs. [2, 44]. However,

for applications it is much more convenient to use the asymptotic form of this expression:

$$\Pi_{el}(h) \approx C \exp(-\kappa h) \qquad \text{for} \quad \exp(-\kappa h) << 1 \tag{5.89}$$

where C is a constant independent of h; as usual, κ is the Debye screening parameter. The constant C was determined by Verwey and Overbeek [17] in the following way.

Let us consider a film of two *identical surfaces* and let us deal with a solution of *symmetric electrolyte*: $Z_1 = -Z_2 = Z$. Combining the Boltzmann equation (5.85) with Eq. (5.80), and expanding in series, one obtains

$$\Pi_{el} = 2n_0 kT \left[\cosh\left(\frac{Ze\psi_m}{kT} \right) - 1 \right] \approx n_0 kT \left(\frac{Ze\psi_m}{kT} \right)^2 \tag{5.90}$$

where $\psi_m \equiv \psi(0)$ is the potential in the middle of the film (Fig. 5.9b), which is assumed to be small:

$$\left(\frac{Ze\psi_m}{kT} \right)^2 << 1 \tag{5.91}$$

Note that we have set $\psi = 0$ in the bulk of solution, see Eq. (5.85); hence small ψ_m means a *weak overlap* of the two double electric layers in the middle of the film. In such case one can use the superposition approximation, $\psi_m \approx 2\psi_1$, that is the potential in the middle of the film is equal to two times the potential at a distance $h/2$ from a single surface, see Fig. 5.9b for the notation. Since ψ_1 is also a small quantity, with the help of Eq. (1.65) one obtains

$$\psi_m \approx 2\psi_1 = 8 \frac{kT}{Ze} \tanh\left(\frac{Ze\psi_s}{4kT} \right) \exp\left(-\frac{\kappa h}{2} \right) \tag{5.92}$$

where ψ_s is the value of the electric potential at the surface of the film. The substitution of Eq. (5.92) into Eq. (5.90) yields [17]

$$\Pi_{el}(h) \approx 64 n_0 kT \left(\tanh \frac{Ze\psi_s}{4kT} \right)^2 \exp(-\kappa h) \qquad \text{for} \quad \exp(-\kappa h) << 1 \tag{5.93}$$

By integration of Eq. (5.93) one can derive expressions for the free energy (per unit area) due to the electrostatic interaction, $f_{el}(h)$, as well as the interaction energy between two bodies, $U_{el}(h_0)$,

with the help of Eqs. (5.9) and (5.49)–(5.52). It is interesting to note, that when ψ_s is large enough, the hyperbolic tangent in Eq. (5.93) is identically 1 and Π_{el} (as well as f_{el} and U_{el}) becomes independent of the surface potential (or charge).

Equation (5.93) can be generalized for the case of *2:1 electrolyte* (divalent counterion) and *1:2 electrolyte* (divalent coion) [94]:

$$\Pi_{el} = 432 n_{(2)} kT \left(\tanh \frac{v_{i:j}}{4} \right)^2 \exp(-\kappa h) \tag{5.94}$$

where $n_{(2)}$ is the concentration of the divalent ions, the subscript "i:j" takes value "2:1" or "1:2", and

$$v_{2:1} = \ln\left[3 / \left(1 + 2\exp\left(-\frac{e\psi_s}{kT} \right) \right) \right], \qquad v_{1:2} = \ln\left[\left(2\exp\left(\frac{e\psi_s}{kT} \right) + 1 \right) / 3 \right] \tag{5.95}$$

Equation (5.93) can be generalized also for the case of two *non-identically* charged interfaces of surface potentials ψ_{s1} and ψ_{s2} for Z:Z electrolytes [2]

$$\Pi_{el}(h) = 64 n_0 kT \gamma_1 \gamma_2 \exp(-\kappa h), \qquad \gamma_k \equiv \tanh\left(\frac{|Z| e\psi_{sk}}{4kT} \right), \qquad k = 1,2 \tag{5.96}$$

Equations (5.93)–(5.96) are valid for both low and high surface potentials, if only $\exp(-\kappa h) << 1$. The comparison of these equations with Eq. (5.89) allow one to determine the parameter C for each specific system. In addition, the expression for the total interaction energy $U = U_{vw} + U_{el}$ can be used to predict the critical electrolyte concentration for coagulation in a colloid, see e.g. Ref. [3, 44]. Likewise, one can determine the critical concentration of electrolyte which is needed for colloid particles to adhere to an interface with the same sign of the surface charge.

5.2.5. *Repulsive hydration force*

The DLVO theory predicts that the height of the electrostatic barrier (see Fig. 5.3) decreases with the increase of the electrolyte concentration in solution. In other words, the added electrolyte suppresses the electrostatic repulsion. In contrast, the experiment [95-98] shows that sometimes at higher electrolyte concentrations (above c.a. 10^{-3} M) a strong repulsive force is

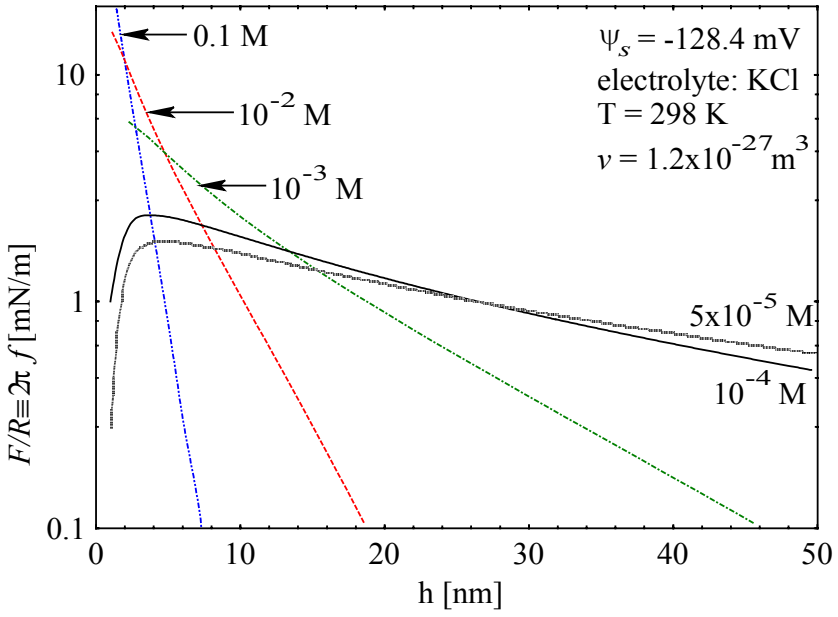

Fig. 5.10. (a) Theoretical dependence of $F/R \equiv 2\pi f$ on the film thickness h for various concentrations of KCl, denoted in the curves. For all curves the surface potential is $\psi_s = -128$ mV, the temperature is 298 K and the excluded volume per ion is $v = 1.2 \times 10^{-27}$ m^3; results from Ref. [100].

detected, which completely dominates the effect of the van der Waals attraction at *short* distances ($h < 10$ nm), see Fig. 5.10. This repulsive interaction is called the *hydration force*. It appears as a deviation from the DLVO theory for short distances between two molecularly smooth electrically charged surfaces. {Note that sometimes other, different effects are also termed "hydration force", see Ref. [99] for review.}

Experimentally the existence of hydration repulsive force was established by Israelachvili *et al*. [95, 96] and Pashley [97, 98] who examined the validity of DLVO-theory at small film thickness in experiments with films from aqueous electrolyte solutions confined between two mica surfaces. At electrolyte concentrations below 10^{-4} M (KNO_3 or KCl) they observed the typical DLVO maximum, However, at electrolyte concentrations higher than 10^{-3} M they did not observe the expected DLVO maximum; instead a strong short range repulsion was detected; cf. Fig. 5.10. Empirically, the hydration force appears to follow an exponential law [3]:

$$f_{\text{hydr}} = f_0 \exp(-h/\lambda_0) \tag{5.97}$$

where, as usual, h is the film thickness; the decay length is $\lambda_0 \approx 0.6 - 1.1$ nm for 1:1 electrolytes; the pre-exponential factor, f_0, depends on the specific surface but is usually about $3 - 30$ mJ/m^2.

The hydration force stabilizes thin liquid films and dispersions preventing coagulation in the primary minimum (that between points 2 and 3 in Fig. 5.3). In historical plan, the hydration repulsion has been attributed to various effects: solvent polarization and H-bonding [101], image charges [102], non-local electrostatic effects [103], existence of a layer of lower dielectric constant, ε, in a vicinity of the interface [104, 105]. It seems, however, that the main contribution to the hydration repulsion between two charged interfaces originates from the *finite size* of the hydrated counterions confined into a narrow subsurface potential well [100]. (The latter effect is not taken into account by the DLVO theory, which deals with *point* ions.) Indeed, in accordance with Eq. (1.65), at high electrolyte concentration (large κ) and not too low surface potential ψ_s, a narrow potential well is formed in a vicinity of the surface, where the concentration of the *counterions* is expected to be much higher than its bulk value. At such high subsurface concentrations (i) the *volume exclusion* effect, due to the finite ionic size, becomes considerable and (ii) the *counterion binding* (the occupancy of the Stern layer) will be greater, see Fig. 1.4. The formed dense subsurface layers from hydrated counterions prevent two similar surfaces from adhesion upon a close contact.

This is probably the explanation of the experimental results of Healy et al. [106], who found that even high electrolyte concentrations cannot cause coagulation of amphoteric latex particles due to binding of strongly hydrated Li^+ ions (of higher effective volume) at the particle surfaces. If the Li^+ ions are replaced by weakly hydrated Cs^+ ions (of smaller effective volume), the hydration repulsion becomes negligible, compared with the van der Waals attraction, and the particles coagulate as predicted by the DLVO-theory.

The effect of the *volume excluded by the counterions* becomes important in relatively thin films, insofar as the aforementioned potential well is located in a close vicinity of the film surfaces. In Ref. [100] this effect was taken into account by means of the Bikerman equation [107, 108]:

$$n_i(z) = \frac{1-v\sum_k n_k(z)}{1-v\sum_k n_{k0}}\, n_{i0}\exp U_i; \qquad U_i = -\frac{Z_i e\psi}{kT} \tag{5.98}$$

Here z is the distance to the charged surface, n_i and U_i are the number density and the potential energy (in kT units) of the i-th ion in the double electric layer; n_{i0} is the value of n_i in the bulk solution; the summation is carried out over all ionic species; v has the meaning of an average excluded volume per counterion; the theoretical estimates [100] show that v is approximately equal to 8 times the volume of the hydrated counterion.

The volume exclusion effect leads to a modification of the Poisson equation (5.86); it is now presented in the form

$$-\frac{\varepsilon}{4\pi}\frac{d^2\psi}{dz^2} = \frac{\sum_i Z_i e n_i^* \exp U_i}{1+v\sum_i n_i^* \exp U_i} \equiv \rho(z); \qquad n_i^* \equiv \frac{n_{i0}}{1+v\sum_k n_{k0}} \tag{5.99}$$

where $\rho(z)$ denotes the charge density in the electric double layer. For $v = 0$ Eq. (5.99) reduces to the expression used in the conventional DLVO theory. Taking into account the definition of U_i, one can numerically solve Eq. (5.99). Next, the total electrostatic disjoining pressure can be calculated by means of the expression [328]

$$\Pi_{\text{el}}^{\text{tot}} \equiv -\int_0^{\psi_m} \rho_m d\psi = \frac{kT}{v}\ln\left[\frac{1+v\sum_k n_k^* \exp\left(-Z_k e\psi_m / kT\right)}{1+v\sum_k n_k^*}\right] \tag{5.100}$$

where the subscript "m" denotes values of the respective variables at the midplane of the film. Finally, the non-DLVO *hydration* force can be determined as an excess over the conventional DLVO electrostatic disjoining pressure:

$$\Pi_{\text{hydr}} \equiv \Pi_{\text{el}}^{\text{tot}} - \Pi_{\text{el}}^{\text{DLVO}} \tag{5.101}$$

where $\Pi_{\text{el}}^{\text{DLVO}}$ is defined by Eq. (5.80), which can be deduced from Eq. (5.100) for $v \to 0$. The effect of $v \neq 0$ leads to a larger value of ψ_m, which contributes to a positive (repulsive) Π_{hydr}. Similar, but quantitatively much smaller, is the effect of the lowering of the dielectric constant,

ε, in a vicinity of the interface [100].

The quantitative predictions of Eqs. (5.99)–(5.101) are found to agree well with experimental data of Pashley [97, 98], Claesson et al. [109] and Horn et al. [110]. In Fig. 5.10 results from theoretical calculations for $F/R \equiv 2\pi f$ vs. h are presented; here F is the force measured by the surface force apparatus between two crossed cylinders of radius R; as usual, f is the total surface free energy per unit area, see Eq. (5.9). The dependence of hydration repulsion on the concentration of electrolyte, KCl, is investigated. All theoretical curves are calculated for $v = 1.2 \times 10^{-27}$ m^3 (8 times the volume of the hydrated K^+ ion), $A_H = 2.2 \times 10^{-20}$ J and $\psi_s = -128.4$ mV; the boundary condition of constant surface potential is used. In Fig. 5.10 for $C_{el} = 5 \times 10^{-5}$ and 10^{-4} M a typical DLVO maximum is observed. However, for $C_{el} = 10^{-3}$, 10^{-2} and 10^{-1} M maximum is not seen, but instead, the short range hydration repulsion appears. These predictions agree with the experimental findings. Note that the increased electrolyte concentration increases the hydration repulsion, but suppresses the long-range double layer repulsion.

5.2.6. *Ion-correlation surface force*

The positions of the ions in an electrolyte solution are correlated in such a way that a *counterion atmosphere* appears around each ion thus screening its Coulomb potential. The latter effect has been taken into account in the theory of strong electrolytes by Debye and Hückel [111, 112], which explains why the activities of the ions in solution are smaller than their concentrations, see Refs. [113, 114] for details. The energy of formation of the counterion atmospheres gives a contribution to the free energy of the system called *correlation energy* [115]. The correlation energy provides a contribution to the osmotic pressure of the electrolyte solution, which can be expressed in the form [111, 112]

$$\Pi_{osm} = kT \sum_{i=1}^{k} n_i - \frac{kT\kappa^3}{24\pi} \tag{5.102}$$

The first term in the right-hand side of the Eq. (5.102) corresponds to an *ideal* solution, whereas the seconds term takes into account the effect of electrostatic *interactions* between the ions. The expression for Π_{el} in the DLVO-theory, Eq. (5.80), obviously corresponds to an ideal

solution, that is to the first term in Eq. (5.102), the contribution of the ionic correlations being neglected.

In the case of overlap of two electric double layers, formed at the surfaces of two bodies interacting across an aqueous phase, the effect of the ionic correlations also gives a contribution, Π_{cor}, to the net disjoining pressure, as pointed out by Guldbrand et al. [116]. Π_{cor} can be interpreted as a surface excess of the last term in Eq. (5.102). In other words, the ionic correlation force originates from the fact that the counterion atmosphere of a given ion in a thin film is different from that in the bulk of the solution. There are two reasons for this difference: (i) the ionic concentration in the film differs from that in the bulk and (ii) the counterion atmospheres are affected (deformed) due to the neighborhood of the film surfaces.

Both numerical [116-118] and analytical [119, 120] methods have been developed for calculating the *ion-correlation component* of disjoining pressure, Π_{cor}. Attard et al. [119] derived the following asymptotic formula, which is applicable to the case of symmetric (*Z*:*Z*) electrolyte and sufficiently thick films [$\exp(-\kappa h) << 1$]:

$$\Pi_{cor} = A_{cor}\Pi_{el} + O\left(e^{-\kappa h}\right), \qquad A_{cor} \equiv \frac{Z^2 e^2 \kappa}{4\varepsilon kT}\left(\ln 2 + 2I_C\right) \tag{5.103}$$

Here Π_{el} is the conventional DLVO electrostatic disjoining pressure, see Eq. (5.80), and

$$I_C = \frac{1}{2}(1+J)\ln 2 + \frac{2-2s^3+s}{2s\left(2s^2-1\right)^2} - \frac{1}{2}(1-J)\ln\left(s+s^2\right) - \frac{\sqrt{s^2-1}}{s}\left[1+J+4\left(2s^2-1\right)^{-3}\right]\arctan\sqrt{\frac{s-1}{s+1}}$$

$$J \equiv \frac{2s^2-3}{\left(2s^2-1\right)^3}, \qquad s \equiv \left[1+\left(\frac{2\pi e\rho_s}{\varepsilon kT\kappa}\right)^2\right]^{1/2}$$

ρ_s is the surface charge density, i.e. the net surface electric charge per unit area.

The theory [117-120] predicts that for films of identically charged surfaces Π_{cor} is *negative* ($A_{cor} < 0$) and corresponds to *attraction*, which can be comparable by magnitude with Π_{vw}. In the case of 1:1 electrolyte Π_{cor} is usually a small correction to Π_{el}. In the case of 2:2 electrolyte, however, the situation can be quite different: for electrolyte concentrations above a certain *critical* value the ion-correlation attraction could become greater than the double layer

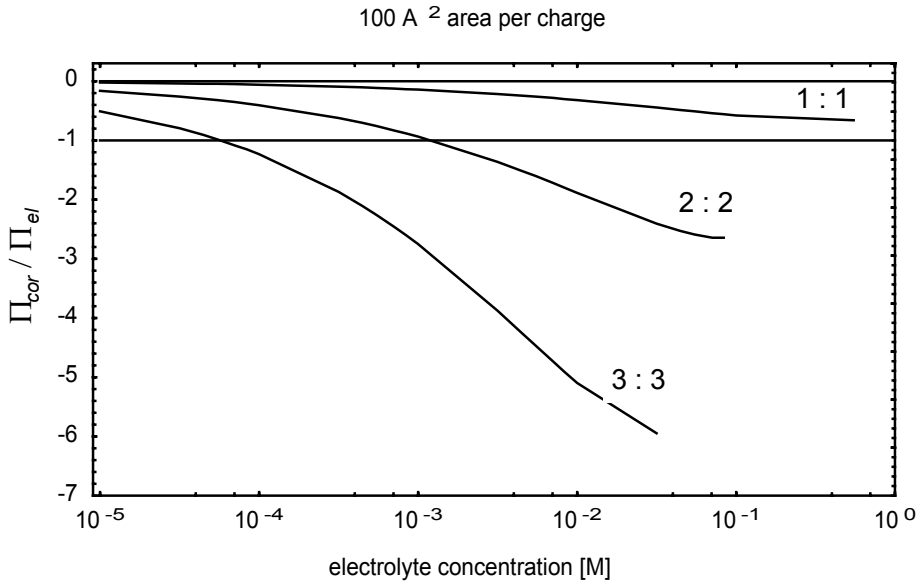

Fig. 5.11. Theoretical dependence of Π_{cor}/Π_{el} on the electrolyte concentration for 1:1, 2:2 and 3:3 electrolytes calculated by means of Eq. (5.103); for all curves the area per surface charge is $|e/\rho_s| = 100$ Å^2; after Ref. [121].

repulsion. In other words, in the presence of bivalent and multivalent counterions Π_{cor} could become the predominant surface force.

To illustrate the theoretical predictions, in Fig. 5.11 we present numerical data computed by means of Eq. (5.103). At constant ρ_s the coefficient A_{cor}, multiplying Π_{el} in Eq. (5.103), is independent of the film thickness h. In other words, for $\exp(-\kappa h) << 1$, the ratio Π_{cor}/Π_{el} is independent of h. In Fig. 5.11 we plot Π_{cor}/Π_{el} vs. the electrolyte concentration for 1:1, 2:2 and 3:3 electrolytes; we have used the value $|e/\rho_s| = 100$ Å^2 for the area per surface charge. The "critical" electrolyte concentration corresponds to the intersection points of the curves with the horizontal line at -1 in Fig. 5.11; for electrolyte concentrations above the critical one the calculated ionic correlation attraction becomes greater by magnitude than the double layer repulsion. One sees in the figure that for a 2:2 electrolyte the critical concentration is about 1 mM, whereas for a 3:3 electrolyte it is below 10^{-4} M.

In the case of secondary thin liquid films, stabilized by ionic surfactant ($h = h_2$ in Fig. 5.3), the measured contact angle is considerably larger than the theoretical value predicted if only van der Waals attraction is taken into account [122]. The experimentally detected additional

attraction in these very thin films ($h \approx 5$ nm) can be attributed to short range ionic correlation effects [123] as well as to the discreteness of the surface charge [2, 124, 125].

Short-range net attractive ion-correlation forces have been measured by Marra [126, 127] and Kjellander et al. [128, 129] between highly charged anionic bilayer surfaces in $CaCl_2$ solutions. These forces are believed to be responsible for the strong adhesion of some surfaces (clay and bilayer membranes) in the presence of divalent counterions [128, 130]. On the other hand, Kohonen et al. [131] measured a monotonic repulsion between two mica surfaces in 4.8×10^{-3} M solution of $MgSO_4$; the lack of attractive surface force in the latter experiments could be attributed, at least in part, to the presence of a strong hydration repulsion due to the Mg^{2+} ions. Additional work is necessary to verify the theoretical predictions and to clarify the physical significance of the ion-correlation surface force.

In summary, the conventional electrostatic disjoining pressure, $\Pi_{el} \equiv \Pi_{el}^{DLVO}$, corresponds to a mean-field model, i.e. *ideal* solution of *point* ions in the electric field of the double layer. The hydration and ionic-correlation components of disjoining pressure, Π_{hydr} and Π_{cor}, represent "superstructures" over the conventional DLVO model of the double-layer forces. In particular, Π_{hydr} takes into account the effect of the ionic *finite volume*. In addition, Π_{cor}, accounts for the *non-ideality* of the electrolyte solutions, which is caused by the long-range electric forces between the ions. The total surface force, due to the overlap of electric double layers, is equal to the sum of the aforementioned three contributions:

$$\Pi_{el}^{tot} = \Pi_{el} + \Pi_{hydr} + \Pi_{cor} \tag{5.104}$$

Note that in view of Eq. (5.89) and (5.103) one obtains

$$\Pi_{el} + \Pi_{cor} = (1 + A_{cor})\Pi_{el} \approx (1 + A_{cor})C \exp(-\kappa h) \equiv \widetilde{C} \exp(-\kappa h)$$

where $\widetilde{C}$ is a "renormalized" pre-exponential factor. In practice $\widetilde{C}$ is determined from the experimental fits and it is often identified with the pre-exponential factor in Eq. (5.93). Thus an apparent (lower) value of the surface potential ψ_s is determined neglecting the effect of the ionic correlations. Of course, this would be correct if $|A_{cor}| << 1$. It turns out that the contribution of the ionic correlations can be detected if only an independently determined value

of ψ_s is available. However, in the case of strong ionic correlations one could have $1 + A_{cor} < 0$, that is $\Pi_{cor}/\Pi_{el} < -1$ in Fig. 5.11; in such a case the net interaction between similar surfaces would become attractive and the effect of Π_{cor} could not be misinterpreted as Π_{el} at lower surface potential.

5.2.7. OSCILLATORY STRUCTURAL AND DEPLETION FORCES

Oscillatory structural forces are observed in two cases:

(i) In very thin liquid films ($h \leq 5$ nm) between two molecularly smooth *solid* surfaces; in this case the period of oscillations is of the order of the diameter of the *solvent* molecules. These, so called *solvation forces* [3, 40], could be important for the short-range interactions between solid particles in dispersions.

(ii) In thin liquid films containing colloidal particles (including surfactant micelles, protein globules, latex beads); in this case the period of the oscillatory force is close to the diameter of the colloid particles, see Fig. 5.12. At higher particle concentrations these *colloid structural forces* stabilize the liquid films and colloids [132-135]. At lower particle concentrations the structural forces degenerate into the so called *depletion attraction*, which is found to destabilize various dispersions [136-138].

In all cases, the oscillations decay with the increase of the film thickness; in the experiment one rarely detects more than 8-9 oscillations.

Physical origin of the oscillatory force. The oscillatory structural force appears when monodisperse spherical (in some cases ellipsoidal or cylindrical) particles are confined between the two surfaces of a thin film. Even one "hard wall" can induce ordering among the neighboring molecules. The oscillatory structural force is a result of overlap of the structured zones formed at two approaching surfaces, see Fig. 5.13 and Refs. [3, 139-141].

A wall can induce structuring in the neighboring fluid only if the magnitude of the surface roughness is negligible compared with the particle diameter, d. If surface irregularities are present (say a rough solid surface), the oscillations are smeared out and oscillatory structural force does not appear. If the film surfaces are fluid, the role of the surface roughness is played

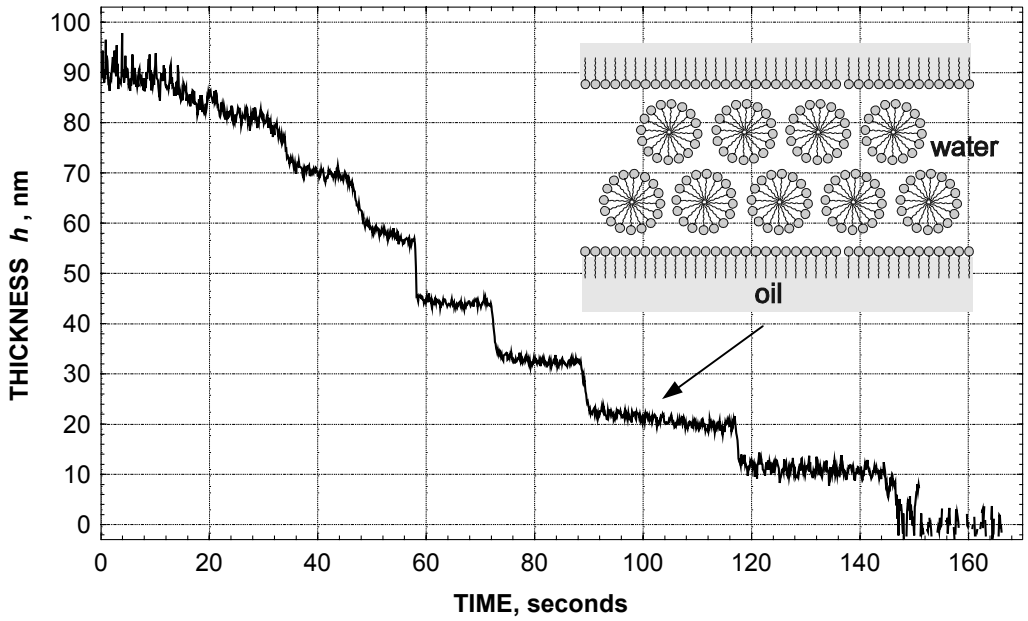

Fig. 5.12. Experimental curve: thickness of an emulsion film, h, vs. time; the step-wise thinning of the film is clearly seen. The film is formed from micellar aqueous solution of the ionic surfactant sodium nonylphenol-polyoxyethylene-25 sulfate (SNP25S) with 0.1 M NaCl; the height of a step is close to the micelle hydrodynamic diameter. The steps represent metastable states corresponding to different number micelle layers inside the film, see the inset; data from Marinova et al. [149].

by the interfacial fluctuation capillary waves, whose amplitude (1–5 Å) is comparable with the diameter of the solvent molecules. Structural forces in foam or emulsion films appear if the diameter of the colloidal particles is much larger than the amplitude of the surface corrugations. Surfactant micelles can play the role of such particles; in fact the manifestation of colloid structural forces was first observed with foam films formed from micellar surfactant solutions.

Johnott [142] and Perrin [143] observed that the thickness of *foam* films decreases with several step-wise transitions. This phenomenon was called "stratification". Bruil and Lyklema [144] and Friberg et al. [145] studied systematically the effect of ionic surfactant and electrolyte on the occurrence of the step-wise transitions. Keuskamp and Lyklema [146] suggested that some oscillatory interaction between the film surfaces must be responsible for the observed phenomenon. Kruglyakov et al. [147, 148] and Marinova et al. [149] observed stratification with *emulsion* films, see Fig. 5.12. Stepwise structuring of colloidal particles has been observed also in *wetting* films (with one solid surface) [150].

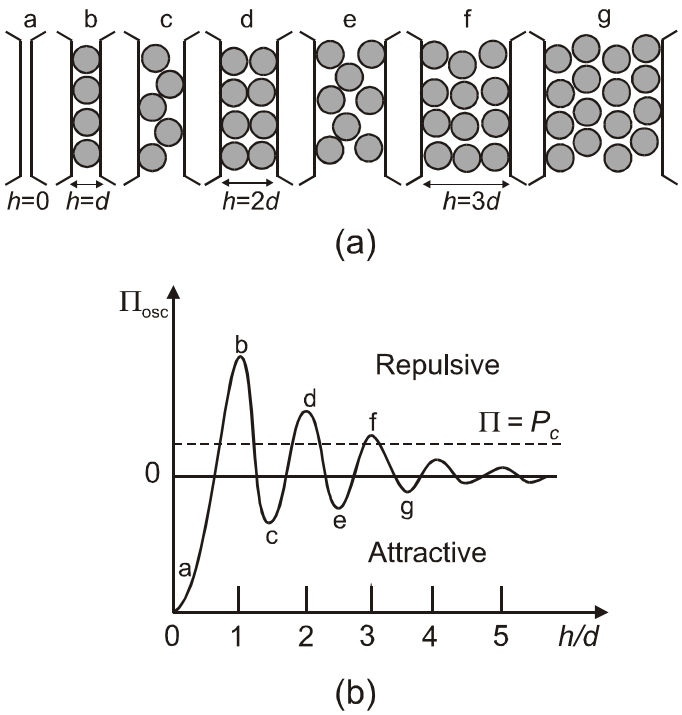

Fig. 5.13. (a) From right to the left: consecutive stages of thinning of a liquid film containing spherical particles of diameter *d*. (b) Schematic plot of the oscillatory-structural component of disjoining pressure, Π_{osc}, vs. the film thickness *h*. The metastable states of the film (the steps in Fig. 5.12) correspond to the intersection points of the oscillatory curve with the horizontal line $\Pi = P_c$, see Eq. (5.3). The stable branches of the oscillatory curve are those with $\partial\Pi/\partial h < 0$; see Ref. [3] for details.

As a first guess, it has been suggested [148, 151] that a possible explanation of the phenomenon can be the formation of surfactant lamella liquid-crystal structure inside the film. Such lamellar micelles are observed to form in surfactant solutions, however, at concentrations much higher than those used in the experiments with stratifying films. The latter fact makes the explanation with lamella liquid crystal irrelevant. Nikolov et al. [41, 132-135] observed stratification not only with micellar surfactant solutions but also with suspensions of latex particles of micellar size. The step-wise changes in the film thickness were approximately equal to the diameter of the spherical particles, contained in the foam film. The observed multiple step-wise decrease of the film thickness (see Fig. 5.12) was attributed to the layer-by-layer thinning of a colloid-crystal-like structure from spherical particles inside the film, which is manifested by the appearance of an oscillatory structural force [133]. The metastable states of the film (the steps) correspond to the roots of the equation $\Pi(h) = P_c$ for the *stable* oscillatory branches with

$\partial\Pi/\partial h < 0$; in Fig. 5.13 there are three such roots; cf. Figs. 5.3 and 5.13; P_c is the applied capillary pressure.

The mechanism of stratification was studied theoretically in Ref. [152], where the appearance and expansion of black spots in horizontal stratifying films was described as a process of condensation of *vacancies* in a colloid crystal of ordered particles within the film. This mechanism was confirmed by subsequent experimental studies with casein submicelles and silica particles [153, 154]. Additional studies with vertical liquid films containing latex particles indicated that the packing of the structured particles is *hexagonal* [155].

The stable branches of the oscillatory disjoining pressure isotherm were experimentally detected for films from micellar solutions by Bergeron and Radke [156]. Oscillatory structural forces due to micelles and microemulsion droplets were directly measured by means of a surface force balance [157, 158]. Static and dynamic light scattering methods were also applied to investigate the micelle structuring in stratifying films [159].

Theoretical expressions for the oscillatory forces. As already mentioned, the period of the oscillations is close to the particle diameter. In this respect the structural forces are appropriately called the "volume exclusion forces" by Henderson [160], who derived an explicit (though rather complex) analytical formula for calculating these forces. Modeling by means of the integral equations of statistical mechanics [161-164] and numerical simulations [165-167] of the oscillatory force of the step-wise film thinning are also available. A convenient semiempirical formula for the oscillatory structural component of disjoining pressure was proposed [168]

$$\begin{aligned} \Pi_{\mathrm{osc}}(h) &= P_0 \cos\left(\frac{2\pi h}{d_1}\right) \exp\left(\frac{d^3}{d_1^2 d_2} - \frac{h}{d_2}\right) \quad \text{for } h>d, \\ &= -P_0 \qquad\qquad\qquad\qquad\qquad\quad \text{for } 0<h<d \end{aligned} \tag{5.105}$$

where d is the diameter of the hard spheres, d_1 and d_2 are the period and the decay length of the oscillations which are related to the particle volume fraction, φ, as follows [168]

$$\frac{d_1}{d} = \sqrt{\frac{2}{3}} + 0.237\,\Delta\varphi + 0.633\,(\Delta\varphi)^2; \qquad \frac{d_2}{d} = \frac{0.4866}{\Delta\varphi} - 0.420 \tag{5.106}$$

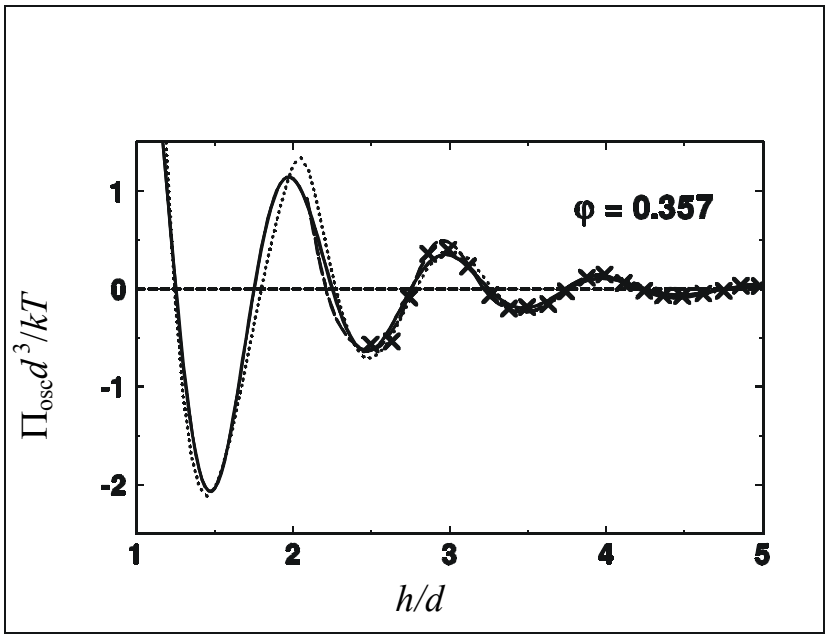

Fig. 5.14. Plot of the dimensionless oscillatory disjoining pressure, $\Pi_{osc}d^3/kT$, vs. the dimensionless film thickness h/d for volume fraction $\varphi = 0.357$ of the particles in the bulk suspension. The solid curve is calculated from Eq. (5.105), the dotted curve – from the theory by Henderson [160], the dashed curve is from Ref. [162] and the ×-points – from Ref. [165]; after Ref. [168].

Here $\Delta\varphi = \varphi_{max} - \varphi$ with φ_{max} being the value of φ at close packing: $\varphi_{max} = \pi/(3\sqrt{2}) \approx 0.74$. P_0 is the particle osmotic pressure determined by means of the Carnahan-Starling formula [169]

$$P_0 = n\,k\,T\,\frac{1+\varphi+\varphi^2-\varphi^3}{(1-\varphi)^3}, \qquad n = \frac{6\varphi}{\pi d^3}, \tag{5.107}$$

where n is the particle number density. For $h < d$, when the particles are expelled from the slit into the neighboring bulk suspension, Eq. (5.105) describes the so called *depletion attraction*, see the first minimum in Fig. 5.13. On the other hand, for $h > d$ the structural disjoining pressure oscillates around P_0, defined by Eq. 5.107. As seen in Fig. 5.14, the quantitative predictions of Eq. (5.105) compare well with the Henderson theory [160] as well as with numerical results Kjellander and Sarman [162] and Karlström [165].

It is interesting to note that in oscillatory regime the concentration dependence of Π_{osc} is dominated by the decay length d_2 in the exponent, cf. Eq. (5.106). Roughly speaking, for a

given distance h the oscillatory disjoining pressure Π_{osc} increases five times when φ is increased with 10%, see Ref. [168].

The contribution of the oscillatory structural forces to the interaction free energy per unit area of the film can be obtained by integrating Π_{osc} in accordance with Eq. (5.9):

$$\begin{aligned} f_{osc}(h) &= \int_h^\infty \Pi_{osc}(h')dh' = F(h), \qquad \text{for } h \geq d \\ &= F(d) - P_0(d-h), \qquad \text{for } 0 \leq h \leq d \end{aligned} \tag{5.108}$$

$$F(h) \equiv \frac{P_0 d_1 \exp\left[\left(d^3/d_1^2 d_2\right) - \left(h/d_2\right)\right]}{4\pi^2 + \left(d_1/d_2\right)^2}\left[\frac{d_1}{d_2}\cos\left(\frac{2\pi h}{d_1}\right) - 2\pi\sin\left(\frac{2\pi h}{d_2}\right)\right]$$

If the colloidal particles are not real hard spheres, then their effective hard-core diameter can be estimated from the formula [134]

$$d \approx [3\beta_2/(4\pi)]^{1/3} \tag{5.109}$$

Where β_2 is the second virial coefficient in the virial expansion of the osmotic pressure due to the particles, $P_{osm}/(nkT) = 1 + \beta_2 n/2 + ...$; β_2 can be determined by static light scattering [170]. In the case of electrically charged particles the effective diameter can be estimated from the expression [132]

$$d \approx d_H + 2\kappa^{-1} \tag{5.110}$$

where d_H is the hydrodynamic diameter of the colloid particles, which can be determined by dynamic light scattering [171].

Depletion interaction. With the decrease of particle (micelle) volume fraction φ the amplitude of the oscillations decreases and the oscillatory structural force degenerates into the depletion interaction (only the first minimum in the oscillatory curve in Fig. 5.13b remains). The latter interaction manifested itself in the experiments by Bondy [172], who observed coagulation of rubber latex in presence of polymer molecules in the disperse medium. In the case of plane-parallel films the depletion component of disjoining pressure is

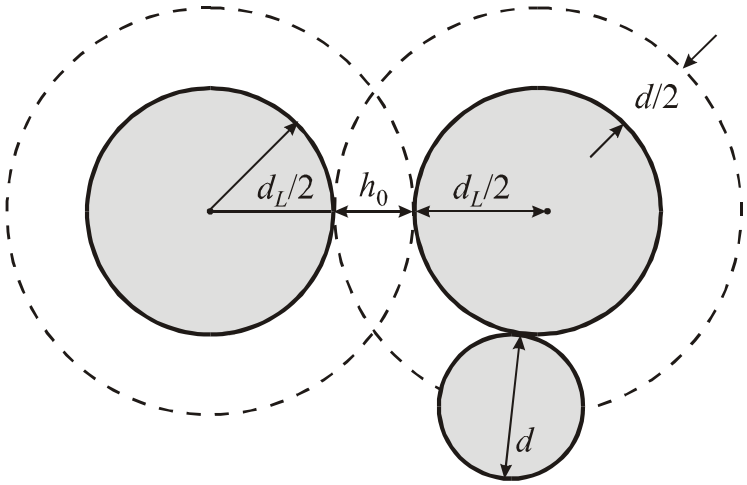

Fig. 5.15. Schematic presentation of the overlap of the depletion zones around two larger particles of diameter d_L separated at a distance h_0. The centers of the smaller particles (of diameter d) cannot come closer to the larger particles than the circumferences denoted with dashed line.

$$\begin{aligned} \Pi_{\text{dep}}(h) &= -P_0 \quad \text{for} \quad h<d \\ \Pi_{\text{dep}}(h) &= 0 \qquad \text{for} \quad h>d \end{aligned} \tag{5.111}$$

which is a special case of Eq. (5.105) for small d_2, see Ref. [3] for details. Evans and Needham [173] to measured the depletion energy of two interacting bilayer surfaces in a concentrated Dextran solution; their results confirm the validity of Eq. (5.111).

Asakura and Oosawa [136, 137] published a theory, which attributed the observed interparticle attraction to the overlap of the depletion layers at the surfaces of two approaching larger colloid particles, see Fig. 5.15. The centers of the smaller particles, of diameter, d, cannot approach the surface of a larger particle (of diameter d_L) at a distance shorter than $d/2$, which is the thickness of the *depletion layer*. When the two depletion layers overlap (Fig. 5.15) some volume between the large particles becomes inaccessible for the smaller particles. This gives rise to an osmotic pressure, which tends to suck out the solvent between the larger particles thus forcing them against each other. The total depletion force experienced by one of the larger particles is [136, 137]

$$F_{\text{dep}} = -kTnS(h_0) \tag{5.112}$$

where the effective depletion area is

$$\begin{aligned} S(h_0) &= \frac{\pi}{4}(2d_L + d + h_0)(d - h_0) \quad \text{for } 0 \le h_0 \le d \\ S(h_0) &= 0 \qquad\qquad\qquad\qquad\quad \text{for } d \le h_0 \end{aligned} \tag{5.113}$$

Here h_0 is the shortest distance between the surfaces of the larger particles and n is the number density of the smaller particles. By integrating Eq. (5.112) one can derive an expression for the depletion interaction energy between the two larger particles, $U_{\text{dep}}(h_0)$. For $d_L >> d$ this expression reads

$$U_{\text{dep}}(h_0)/kT \approx -\frac{3}{2}\varphi\frac{d_L}{d^3}(d - h_0)^2, \qquad 0 \le h_0 \le d \tag{5.114}$$

where $\varphi = \pi n d^3/6$ is the volume fraction of the small particles. The maximum value of U_{dep} at $h_0 = 0$ is $U_{\text{dep}}(0)/kT \approx -3\varphi d_L/(2d)$. For example, if $d_L/d = 50$ and $\varphi = 0.1$, then $U_{\text{dep}}(0) = -7.5\,kT$. This depletion attraction turns out to be large enough to cause flocculation in dispersions and attachment of particles to surfaces [42, 138, 174-177], as well as attraction between lipid bilayers [178, 179].

5.2.8. STERIC INTERACTION DUE TO ADSORBED MOLECULAR CHAINS

The adsorption of polymeric molecules at an interface may lead to the appearance of polymeric *brushes*, see Fig. 5.16. The polymers could be attached to the surface by chemical bonding (chemisorption, anchoring) of some groups. Alternatively, a polymeric coverage of the surface can be achieved by physical adsorption of nonionic surfactants, whose hydrophilic moieties represent water-soluble polymers (typically – polyoxyethylenes).

When two surfaces covered with polymer brushes approach each other, the overlap of the brushes gives rise to a strong osmotic repulsion, which protects the surfaces from adhesion and the colloidal dispersions from coagulation [3, 42, 180-182]. This *steric repulsion* plays a role similar to that of the electrostatic repulsion with respect to colloid stability.

Thickness of a separate polymeric brush. Obviously, the range of action of the steric repulsion is determined by the thickness of the brush, L. The latter can be defined as the mean-square end-to-end distance of the hydrophilic portion of the chain. If a chain, composed of N

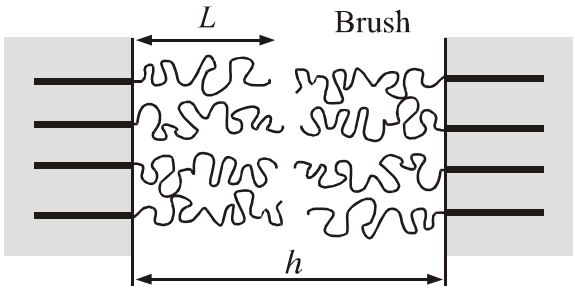

Fig. 5.16. Polymeric chains adsorbed at an interface form a "brush" of thickness L. The overlap of the brushes formed at the two surfaces of a thin liquid film gives rise to a steric interaction.

segments, were completely extended, then L would be equal to lN, where l is the length of a polymeric segment. However, due to the Brownian motion $L < lN$. For an isolated anchored chain in an ideal (theta) solvent L can be estimated as [42]

$$L \approx L_0 \equiv l\sqrt{N} \tag{5.115}$$

The solvent–polymer interactions may essentially influence L, and therefrom – the steric interaction. The osmotic pressure of either dilute or concentrated polymer solutions can be expressed in the form [183]

$$\frac{P_{\text{osm}}}{nkT} = \frac{1}{N} + \frac{1}{2}nv + \frac{1}{3}n^2 w + \ldots \tag{5.116}$$

Here n is the number segment density, v and w account for the pair and triplet interactions between segments. In fact v and w are counterparts of the second and third virial coefficients in the theory of non-ideal gases [114]. v and w can be calculated if information about the polymer chain and the solvent is available [42]

$$w^{1/2} = \bar{v}m / N_A, \qquad v = w^{1/2}(1 - 2\chi), \tag{5.117}$$

where $\bar{v}$ (m^3/kg) is the specific volume per segment, m (kg/mol) is the molecular weight per segment, N_A is the Avogadro number and χ is the Flory parameter [114]:

$$\chi = -\frac{c}{2kT}\left(u_{PP} + u_{SS} - 2u_{PS}\right) \tag{5.118}$$

c is the number of the closest neighbors of a molecule, u_{AB} stands for the energy of interaction

between molecules type *"A"* and *"B"* (*A*,*B* = *P*,*S*; *"P"* = polymeric segment, *"S"* = solvent molecule). The parameter *v* can be zero (see Eq. 5.117) for some special temperature, called the *theta temperature*. The solvent at theta temperature is known as *theta solvent* or *ideal solvent*. At the theta temperature the intermolecular (intersegment) attraction and repulsion in polymer solutions are exactly counterbalanced. In a *good solvent*, however, the repulsion prevails over the attraction and $v > 0$. In contrast, in a *poor solvent* the intersegment attraction prevails, so $v < 0$.

In a good solvent $L > L_0$, whereas in a poor solvent $L < L_0$. In addition, L depends on the surface concentration, Γ, of the adsorbed chains, i.e. L is different for an isolated molecule and for a brush. If the segments repel each other, larger Γ leads to greater L. The mean field approach [42, 184], applied to polymer solutions, provides the following equation for calculating L:

$$\widetilde{L}^3 - \left(1 + \frac{1}{9}\widetilde{\Gamma}^2\right)\widetilde{L}^{-1} = \frac{1}{6}\widetilde{v} \tag{5.119}$$

where $\widetilde{L}, \widetilde{\Gamma}$ and $\widetilde{v}$ are the dimensionless values of L, Γ and v defined as follows:

$$\widetilde{L} = L/\left(l\sqrt{N}\right), \qquad \widetilde{\Gamma} = \Gamma N\sqrt{w}/l, \qquad \widetilde{v} = v\Gamma N^{3/2}/l \tag{5.120}$$

For an isolated adsorbed molecule ($\widetilde{\Gamma} = 0$) in an ideal solvent ($\widetilde{v} = 0$) Eq. (5.119) predicts $\widetilde{L} = 1$, that is $L = L_0$.

Interaction between two overlapping polymeric brushes. As already mentioned, the major source of the steric repulsion between brushes (Fig. 5.16) is the increased osmotic pressure in the zone of overlap. However, two other factors tend to reduce the osmotic repulsion. (i) In a poor solvent the segments of the chain molecules attract each other; hence the overlap of the two approaching layers of polymer molecules will be accompanied with the appearance of more intersegment contacts which will decrease the free energy of the system. The latter effect could sometimes prevail over the osmotic repulsion in the case of small overlap (two brushes just touching each other). However, in the case of larger overlap (smaller *h*) the osmotic repulsion becomes predominant, see Fig. 5.17. (ii) Due to the repulsive

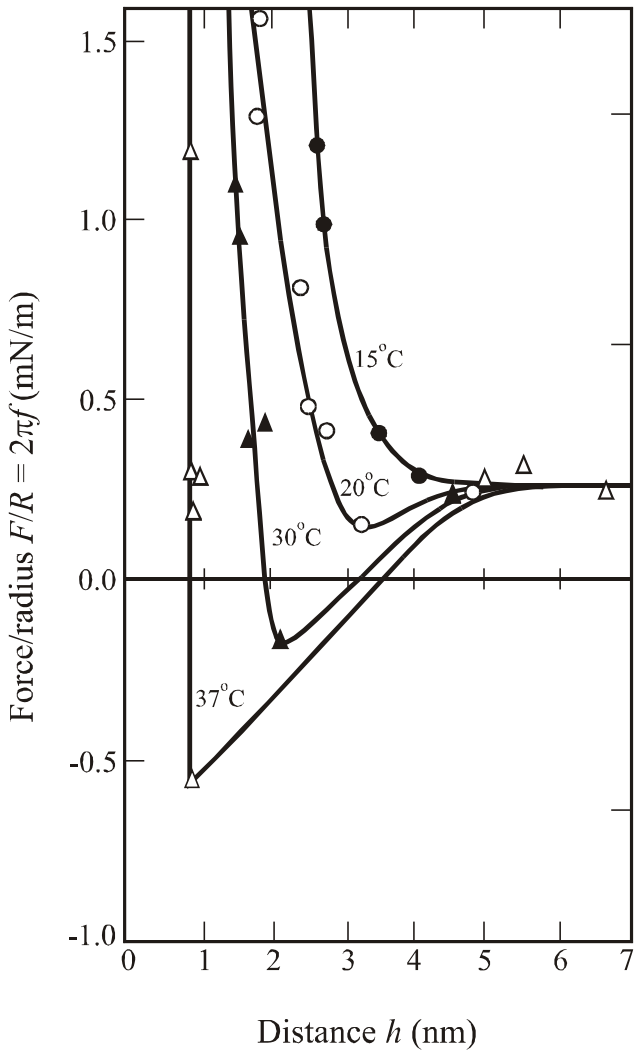

Fig. 5.17. Experimental data for the steric interaction obtained by surface force apparatus. Plot of $F/R \equiv 2\pi f$ vs. h for two surfaces covered with adsorption monolayers from the nonionic surfactant $C_{12}(EO)_6$ for various temperatures. The appearance of minima indicates that with the increase of temperature the water becomes a poor solvent for the polyoxyethylene chains. (From Ref. 190.)

interactions with the chains of neighboring molecules in the brush each polymeric chain is subjected to an extension ($L > L_0$, see Eq. 5.119), which produces an extra elastic stress. This elastic stress can be partially released when two such monolayers are pressed against each other. As a result, the free energy of the system decreases, which is equivalent to an effective attractive contribution to the net steric surface force, which will be briefly termed *elastic attraction*.

Dolan and Edwards [185] calculated the steric interaction free energy per unit area, f_{st}, for two polymeric adsorption monolayers in an *ideal solvent* as a function of the film thickness, h,:

$$f_{st}(h) = \Gamma kT\left[\frac{\pi^2}{3}\frac{L_0^2}{h^2} - \ln\left(\frac{8\pi}{3}\frac{L_0^2}{h^2}\right)\right] \quad \text{for } h < L_0\sqrt{3} \tag{5.121}$$

$$f_{\mathrm{st}}(h) = 4\Gamma kT \exp\left(-\frac{3h^2}{2L_0^2}\right) \qquad \text{for } h > L_0\sqrt{3} \tag{5.122}$$

where L_0 is defined by Eq. (5.115). The first term in the right-hand side of Eq. (5.121) comes from the osmotic repulsion between the brushes; the second term is negative and accounts effectively for the decrease of the elastic energy of the initially extended chains with the decrease of the film thickness, h. The boundary between the power-law regime ($f_{\mathrm{st}} \propto 1/h^2$) and the exponential decay regime is at $h = L_0\sqrt{3} \approx 1.7\,L_0$, the latter being slightly less than $2L_0$ which is the intuitively expected beginning of the steric overlap.

In the case of a *good solvent* the disjoining pressure $\Pi_{\mathrm{st}} = -df_{\mathrm{st}}/dh$ can be calculated by means of an expression stemming from the theory by Alexander and de Gennes [186-188]:

$$\Pi_{\mathrm{st}}(h) = kT\Gamma^{3/2}\left[\left(\frac{2L_{\mathrm{g}}}{h}\right)^{9/4} - \left(\frac{h}{2L_{\mathrm{g}}}\right)^{3/4}\right] \qquad \text{for } h < 2L_{\mathrm{g}}; \qquad L_{\mathrm{g}} = N\left(\Gamma l^5\right)^{1/3} \tag{5.123}$$

where L_{g} is the thickness of a brush in a good solvent [186]. The positive and the negative terms in the right-hand side of Eq. (5.123) correspond to osmotic repulsion and elastic attraction. The validity of Alexander–de Gennes theory was experimentally confirmed by Taunton et al. [189] who measured the forces between two brush layers grafted on the surfaces of two crossed mica cylinders, see also Ref. [3]. Theoretical expressions, which are applicable to the case when intersegment *attraction* is present (the solvent is poor, see Fig. 5.17) are reviewed by Russel et al. [42].

5.2.9. UNDULATION AND PROTRUSION FORCES

Adsorption monolayers at fluid interfaces and bilayers of amphiphilic molecules in solution (phospholipid membranes, surfactant lamellas) are involved in a fluctuation wave motion. The configurational confinement of such thermally exited modes within the narrow space between two approaching interfaces gives rise to short-range repulsive surface forces, called *fluctuation forces*, which are briefly presented below.

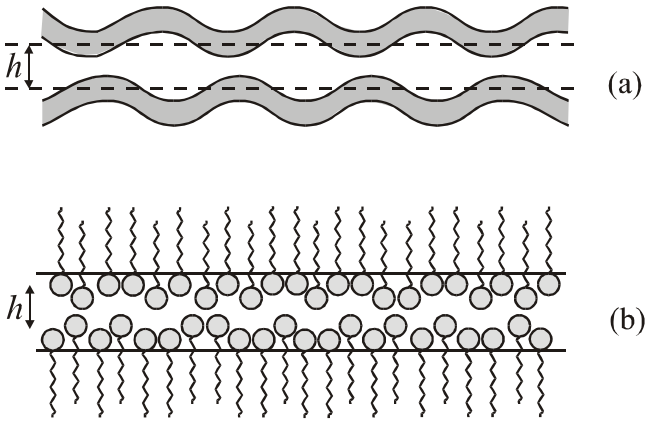

Fig. 5.18. Fluctuation wave forces due to configurational confinement of thermally excited modes into a thin liquid film. (a) The undulation force is related to the bending mode of membrane fluctuations. (b) The protrusion force is caused by the spatial overlap of protrusions of adsorbed amphiphilic molecules.

Undulation force. The undulation force arises from the configurational confinement related to the bending mode of deformation of two fluid bilayers, like surfactant lamellas or lipid membranes. This mode consists in undulation of the bilayer at constant area and thickness, Fig. 5.18a. Helfrich et al. [191, 192] established that two such undulated "tension-free" bilayers, separated at a mean surface-to-surface distance h, experience a *repulsive* disjoining pressure:

$$\Pi_{\text{und}}(h) = \frac{3\pi^2 (kT)^2}{64 k_t h^3} \tag{5.124}$$

Here k_t is the total bending elastic modulus of the bilayer as a whole; the experiment shows that k_t is of the order of 10^{-19} J for lipid bilayers [193]. The undulation force was measured and the dependence $\Pi_{\text{und}} \propto h^{-3}$ was confirmed experimentally [194-196]. In lamellar phases present in concentrated solutions of nonionic amphiphiles the undulation repulsion opposes the van der Waals attraction thus producing a stabilizing effect [197-199].

Protrusion force. The protrusion of an amphiphilic molecule from an adsorption monolayer (or micelle) may fluctuate about the equilibrium position of the molecule owing to the thermal motion, Fig. 5.18b. In other words, the adsorbed molecules are involved in a *discrete* wave motion, which differs from the continuous mode of deformation related to the

undulation force. The molecular protrusions from lipid membranes and adsorption monolayers have been detected by means of NMR, neutron diffraction and X-ray synchrotron diffraction [200, 201]. In relation to the micelle kinetics, Aniansson et al. [202, 203] found that the energy of protrusion of an amphiphilic molecule can be modeled as a linear function: $u(z) = \alpha z$, where z is the distance out of the surface ($z > 0$); they determined $\alpha \approx 3 \times 10^{-11}$ J/m for single-chained surfactants. By using a mean-field approach Israelachvili and Wennerström [99] derived an expression for the protrusion disjoining pressure which appears when two protrusion zones overlap (Fig. 5.18b):

$$\Pi_{\text{protr}}(h) = \frac{\Gamma kT}{\lambda} \frac{(h/\lambda)\exp(-h/\lambda)}{1-(1+h/\lambda)\exp(-h/\lambda)}, \qquad \lambda \equiv \frac{kT}{\alpha}. \tag{5.125}$$

λ has the meaning of characteristic protrusion decay length; $\lambda = 0.14$ nm at 25°C; Γ denotes the number of protrusion sites per unit area. Π_{protr} is positive and corresponds to *repulsion*; it decays exponentially for $h << \lambda$; in the other limit, $h >> \lambda$, we have $\Pi_{\text{protr}} \propto h^{-1}$, that is Π_{protr} is divergent for $h \to 0$. Integrating Eq. (5.125) in accordance with Eq. (5.9) one obtains a relatively compact expression for the free energy of the protrusion interaction per unit area:

$$f_{\text{protr}}(h) = \int_h^\infty \Pi_{\text{protr}}(\hat{h})\, d\hat{h} = -\Gamma kT \ln[1 - (1 + h/\lambda)\exp(-h/\lambda)] \tag{5.126}$$

5.2.10. FORCES DUE TO DEFORMATION OF LIQUID DROPS

Effect of the interfacial dilatation. In the course of collision of a liquid drop with a solid surface (Fig. 5.19a) or with another drop (Fig. 5.19b) interfacial deformations may happen. We assume that before the collision the fluid particle is sphere of radius R. When the surface-to-surface distance h is sufficiently small, a flattening (a film of radius r_c) could appear in the zone of contact. This deviation from the spherical shape causes a dilatation of the surface of the fluid particle; the respective increase of the surface energy can be deduced as follows.

For small dilatation, $\alpha \equiv dA/A$, the surface tension can be expanded in series: $\sigma = \sigma_0 + E_G\alpha + \cdots$ where σ_0 is the surface tension of the non-deformed drop, A and E_G denote area and Gibbs elasticity, see Eq. (1.145). Then the work of dilatation per unit area is

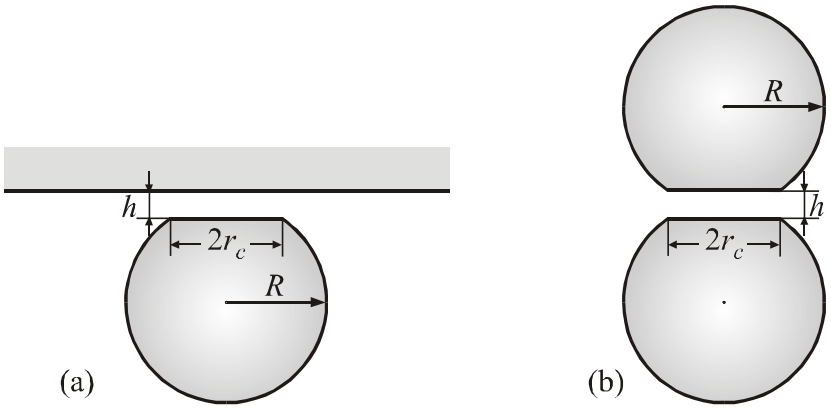

Fig. 5.19. Deformation of interacting emulsion drops: (a) drop colliding with a solid surface; (b) central collision of two drops; R is the radius of the spherical part of the drop; r_c is the radius of the contact line at the boundary film–meniscus.

$$w_{\text{dil}} = \int_0^{\alpha} (\sigma_0 + E_G \alpha) d\alpha = \sigma_0 \frac{\Delta A}{A_0} + \frac{E_G}{2} \left(\frac{\Delta A}{A_0} \right)^2 \tag{5.127}$$

where A_0 is the area if the nondeformed (spherical) drop and $\Delta A = A - A_0$ is the increase of its area upon deformation. The total energy of surface dilatation is [37]

$$U_{\text{dil}} = A_0 w_{\text{dil}} = j \sigma_0 \Delta A + \frac{j}{2} A_0 E_G \left(\frac{\Delta A}{A_0} \right)^2 \tag{5.128}$$

where $j = 1,2$ for the system depicted in Fig. 5.19a and 5.19b, respectively. Further, the surface area and the volume of a deformed drop are

$$A = \pi R^2 (2 + 2\cos\alpha + \sin^2\alpha) \tag{5.129}$$

$$V = \frac{\pi}{3} R^3 (2 + 2\cos\alpha + \sin^2\alpha \cos\alpha) \tag{5.130}$$

where $\sin\alpha = r_c/R$, see Fig. 5.19 for the notation. We consider small deformations at fixed volume of the drop; then using series expansion in Eq. (5.130) for $\varepsilon \equiv \sin^2\alpha << 1$ and fixed V one can derive

$$R^2 = R_0^2\left(1+\frac{\varepsilon^2}{8}+\cdots\right), \qquad R_0 = \left(\frac{3V}{4\pi}\right)^{1/3} \tag{5.131}$$

Substituting Eq. (5.131) into Eq. (5.129) and expanding again in series for small ε one obtains

$$A = A_0 + \Delta A \approx 4\pi R_0^2\left(1+\frac{\varepsilon^2}{16}\right) = A_0 + A_0\left(\frac{r_c}{2R}\right)^4 \qquad (A_0 = 4\pi R_0^2) \tag{5.132}$$

Finally, combining Eqs. (5.128) and (5.132) one deduces [37]

$$U_{\rm dil} = \frac{\pi j}{4}\sigma_0\frac{r_c^4}{R^2} + \frac{\pi j}{128}E_G\frac{r_c^8}{R^6}+\cdots, \qquad (r_c/R)^2 << 1 \tag{5.133}$$

Calculations for typical emulsion systems show that the condition $(r_c/R)^2 << 1$ is always satisfied and Eq. (5.127) holds with a good precision. The contribution of E_G to $U_{\rm dil}$, that is the last term in Eq. (5.133) is usually an effect of higher order and can be neglected. However, for microemulsion drops the surface tension is rather low, $\sigma << 1$ mN/m, and then the term with E_G in Eq. (5.133) may become significant. On the other hand, if there is no adsorbed surfactant on the drop surface, then $E_G = 0$. In all cases $U_{\rm dil} > 0$, i.e. the interfacial dilatation gives rise to an effective repulsion between the two droplets. Equation (5.133) predicts that $U_{\rm dil}$ strongly increases with the rise of the film radius r_c.

Effect of interfacial bending. The flattening of the drop surface in the zone of contact (Fig. 5.19) is accompanied by change in the interfacial bending energy, $U_{\rm bend}$. In Section 3.3.2 we have considered in detail this effect; in agreement with Eq. (3.96) the energy of interfacial bending is [39]:

$$U_{\rm bend} = -j\pi r_c^2 B_0/R, \qquad (r_c/R)^2 << 1 \tag{5.134}$$

where B_0 is the interfacial bending moment, and j is the same as in Eq. (5.128). Note that $B_0 = -4k_cH_0$, where H_0 is the spontaneous curvature and k_c is the interfacial bending elastic modulus. As discussed in Section 3.3.2, for oil-in-water (O/W) emulsions $U_{\rm bend} > 0$ and, consequently, the interfacial bending is energetically unfavorable. However, for water-in-oil (W/O) emulsions $U_{\rm bend} < 0$, which favors the flattening [39].

5.3. SUMMARY

The act of collision of a colloid particle with an interface (or with another particle) is accompanied by the formation of a thin liquid film between the two approaching surfaces. If attractive forces prevail in the liquid film, the latter becomes unstable, breaks and the particle "enters" the interface (or coalesces with the other particle). Conversely, if the repulsive forces are predominant, the particle will rebound from the interface and there will be no attachment / coagulation. A third possibility is the attractive and repulsive forces to counterbalance each other; in such case an equilibrium film is formed between the particle and the interface (the other particle). The balance of all forces exerted on an attached particle is considered, see Fig. 5.2. It turns out that at equilibrium the repulsive forces dominate the *disjoining pressure* Π, which is counterbalanced by the action of *transversal tension* τ, the latter being dominated by the attractive forces in the transition zone film–meniscus, see Eq. (5.13). Thermodynamic relationships of the latter quantities with the *contact angle* are derived. Next we consider the Derjaguin approximation, which allows one to calculate the interaction across a film of nonuniform thickness if the interaction energy per unit area of a plane-parallel film is known, see Eq. (5.46).

Further we consider interactions of different physical origin in thin liquid films. Expressions for the *van der Waals interaction* between particles / interfaces of various shapes are presented, Eqs. (5.57)–(5.64). Equations for calculating the Hamaker constant are reviewed, see Eqs. (5.65)–(5.78). Hypotheses about the nature of the long-range *hydrophobic surface force* and its physical significance are discussed in Section 5.2.3. Special attention is paid to the *electrostatic surface force* which is due to the overlap of the electric double layers formed at the charged surfaces of an aqueous film, Section 5.2.4. A more detailed theory of the interactions across films from electrolyte solutions should take into account also the *hydration repulsion* (Section 5.2.5) and *ion-correlation attraction* (Section 5.2.6). The presence of fine colloidal particles (surfactant micelles, protein globules, etc.) in a liquid film gives rise to an *oscillatory structural force*, which could stabilize the film or cause its step-wise thinning (stratification), Section 5.2.7. At low volume fractions of the fine particles the oscillatory force degenerates to the *depletion attraction*, which leads to particle attachment and flocculation; see Eqs.

(5.111)–(5.114). Adsorbed polymeric molecules form "brushes" at the film surfaces; the overlap of such "brushes" in the course of film thinning produce a *steric interaction*. The latter can be repulsive or attractive depending on whether the water is good or poor solvent for the polymeric chains, see Section 5.2.8. Similar steric–osmotic effects appears when configurational confinement of thermally excited surface modes takes place in a thin liquid film. The bending mode of surface fluctuations gives rise to the *undulation force*, whereas the discrete protrusions of adsorbed amphiphilic molecules lead to the appearance of a short-range *protrusion force*, both of them being repulsive, see Section 5.2.9. Finally, the collisions of emulsion drops are accompanied with deformation, i.e. deviation from the spherical shape, see Fig. 5.19. This causes extension of the drop surface area and change in the surface curvature, which lead to *dilatational* and *bending* contributions to the overall interaction energy, see Eqs. (5.133) and (5.134). The total particle–surface (or particle–particle) interaction energy is a superposition of contributions from all operative surface interactions, see Eq. (5.53).

Another important contribution to the particle-surface and particle-particle interactions stems from the viscous friction in the thin liquid films. This *hydrodynamic interaction* is considered in the next Chapter 6.

5.4. REFERENCES

1. I.B. Ivanov, D.S. Dimitrov, Thin Film Drainage, in: "Thin Liquid Films", I.B. Ivanov (Ed.), Marcel Dekker, New York, 1988; p. 379.
2. B.V. Derjaguin, N.V. Churaev, V.M. Muller, "Surface Forces", Plenum Press: Consultants Bureau, New York, 1987.
3. J.N. Israelachvili, "Intermolecular and Surface Forces", Academic Press, London, 1992.
4. B.V. Derjaguin, E.V. Obuhov, Acta Physicochim. USSR 5 (1936) 1.
5. A.J. Vries, Rec. Trav. Chim. Pays-Bas 77 (1958) 44.
6. A. Scheludko, Proc. K. Akad. Wetensch. B, 65 (1962) 87.
7. A. Vrij, Disc. Faraday Soc. 42 (1966) 23.
8. I.B. Ivanov, B. Radoev, E. Manev, A. Scheludko, Trans. Faraday Soc. 66 (1970) 1262.
9. I.B. Ivanov, D. S. Dimitrov, Colloid Polymer Sci. 252 (1974) 982.
10. A. Hadjiiski, R. Dimova, N.D. Denkov, I.B. Ivanov, R. Borwankar, Langmuir 12 (1996) 6665.
11. S.M. Patrick, H. An, M.B. Harris, I.B. Ivanov, N.S. Braunstein, E.F. Leonard, Annals Biomedical Eng. 25 (1997) 1072.

12. I.B. Ivanov, A. Hadjiiski, N.D. Denkov, T.D. Gurkov, P.A. Kralchevsky, S. Koyasu, Biophys. J. 75 (1998) 545.
13. B.V. Derjaguin, M.M. Kussakov, Acta Physicochim. USSR, 10 (1939) 153.
14. P.A. Kralchevsky, I.B. Ivanov, Chem. Phys. Lett., 121 (1985) 111.
15. P.A. Kralchevsky, I.B. Ivanov, Chem. Phys. Lett., 121 (1985) 116.
16. B.V. Derjaguin, L.D. Landau, Acta Physicochim. USSR 14 (1941) 633.
17. E.J.W. Verwey, J.Th.G. Overbeek, "The Theory of Stability of Lyophobic Colloids", Elsevier, Amsterdam, 1948.
18. D. Exerowa, A. Scheludko, Bull. Inst. Chim. Phys. Bulg. Acad. Sci., 4, (1964) 175.
19. K.J. Mysels, J. Phys. Chem. 68 (1964) 3441.
20. P.M. Kruglyakov, Equilibrium properties of free films and stability of foams and emulsions, in: "Thin Liquid Films", I.B. Ivanov (Ed.), M. Dekker, New York, 1988; p.767.
21. D. Exerowa, P.M. Kruglyakov, "Foam and Foam Films", Elsevier, Amsterdam, 1998.
22. A.D. Nikolov, P.A. Kralchevsky, I.B. Ivanov, A.S. Dimitrov, AIChE Symposium Series No. 252, Vol. 82, American Inst. of the Chemical Engineers, New York, 1986; p. 82.
23. I.B. Ivanov, P.A. Kralchevsky, in: "Thin Liquid Films", I.B. Ivanov (Ed.), Marcel Dekker, New York, 1988; p. 49.
24. K.D. Danov, P.A. Kralchevsky, I.B. Ivanov, in: Encyclopedic Handbook of Emulsion Technology, J. Sjöblom (Ed.), Marcel Dekker, New York, 2001.
25. A.I. Rusanov, "Phase Equilibria and Surface Phenomena", Khimia, Leningrad, 1967 (in Russian); "Phasengleichgewichte und Grenzflächenerscheinungen", Akademie Verlag, Berlin, 1978.
26. G.A. Martynov, B.V. Derjaguin, Kolloidn. Zh. 24 (1962) 480.
27. B.V. Toshev, I.B. Ivanov, Colloid Polym. Sci. 253 (1975), 558.
28. I.B. Ivanov, B.V. Toshev, Colloid Polym. Sci., 253 (1975) 593.
29. A.N. Frumkin, Zh. Phys. Khim. USSR, 12 (1938) 337.
30. J.A. de Feijter, Thermodynamics of Thin Liquid Films, in: "Thin Liquid Films", I.B. Ivanov (Ed.), Marcel Dekker, New York, 1988; p. 1.
31. S. Ono, S. Kondo, Molecular Theory of Surface Tension in Liquids, in: S. Flügge (Ed.), Handbuch der Physik, vol. 10, Springer, Berlin, 1960, p. 134.
32. P.A. Kralchevsky, K.D. Danov, N.D. Denkov, Chapter 11 in "Handbook of Surface and Colloid Chemistry", K.S. Birdi (Ed.), CRC Press, New York, 1997; p. 333.
33. A.S. Dimitrov, P.A. Kralchevsky, A.D. Nikolov, D.T. Wasan, Colloids Surf. 47 (1990) 299.
34. B.V. Derjaguin, Kolloid Zeits. 69 (1934) 155.
35. P. Attard, J. L. Parker, J. Phys. Chem. 96 (1992) 5086.
36. K.D. Danov, N.D. Denkov, D.N. Petsev, R. Borwankar, Langmuir 9 (1993) 1731.
37. K.D. Danov, D.N. Petsev, N.D. Denkov, R. Borwankar, J. Chem. Phys. 99 (1993) 7179.
38. N.D. Denkov, D.N. Petsev, K.D. Danov, J. Colloid Interface Sci. 176 (1995) 189.
39. D.N. Petsev, N.D. Denkov, P.A. Kralchevsky, J. Colloid Interface Sci. 176 (1995) 201.
40. R.G. Horn, J.N. Israelachvili, Chem. Phys. Lett. 71 (1980) 192.

41. A.D. Nikolov, D.T. Wasan, P.A. Kralchevsky, I.B. Ivanov, Ordered Structures in Thinning Micellar Foam and Latex films, in: "Ordering and Organisation in Ionic Solutions", N. Ise and I. Sogami (Eds.), World Scientific, Singapore, 1988; p. 302.
42. W.B. Russel, D.A. Saville, W.R. Schowalter, "Colloidal Dispersions", Cambridge Univ. Press, Cambridge, 1989.
43. I.B. Ivanov, K.D. Danov, P.A. Kralchevsky, Colloids Surf. A 152 (1999) 161.
44. B.V. Derjaguin, "Theory of Stability of Colloids and Thin Liquid Films", Plenum Press: Consultants Bureau, New York, 1989.
45. I.B. Ivanov (Ed.), "Thin Liquid Films", Marcel Dekker, New York, 1988.
46. W.H. Keesom, Proc. Amst. 15 (1913) 850.
47. P. Debye, Physik 2 (1920) 178.
48. F. London, Z. Phys. 63 (1930) 245.
49. F. London, Trans. Faraday Soc. 83 (1937) 8.
50. J. Mahanty, B.W. Ninham, "Dispersion Forces", Academic Press, New York, 1976.
51. H.C. Hamaker, Physics 4 (1937) 1058.
52. S. Nir, C. S. Vassilieff, Van der Waals Interactions in Thin Films" in: "Thin Liquid Films", I.B. Ivanov (Ed.), Marcel Dekker, New York, 1988; p.207.
53. E.M. Lifshitz, Soviet Phys. JETP (Engl. Transl.) 2 (1956) 73.
54. S. Usui, H. Sasaki, F. Hasegawa, Colloids Surf. 18 (1986) 53.
55. T.D. Blake, J. Chem. Soc. Faraday Trans. I, 71 (1975) 192.
56. M.L. Gee, T.W. Healy, L.R. White, J. Colloid Interface Sci. 131 (1989) 18.
57. I.E. Dzyaloshinskii, E.M. Lifshitz, L.P. Pitaevskii, Adv. Phys. 10 (1961) 165.
58. E.S. Sabisky, C. H. Anderson, Phys. Rev. A 7 (1973) 790.
59. H.R. Casimir, D. Polder, Phys. Rev. 73 (1948) 360.
60. B.V. Derjaguin, I.I. Abrikossova, Discuss. Faraday Soc. 18 (1954) 24.
61. J.N. Israelachvili, R.M. Pashley, Nature 300 (1982) 341.
62. Ya.I. Rabinovich, B.V. Derjaguin, N. Churaev, Adv. Colloid Interface Sci. 16 (1982) 63.
63. R.M. Pashley, P.M. McGuiggan, B.W. Ninham, D.F. Evans, Science 229 (1985) 1088.
64. Ya.I. Rabinovich, B.V. Derjaguin, Colloids Surf. 30 (1988) 243.
65. H.K. Christenson, P.M. Claesson, Science 239 (1988) 390.
66. J.L. Parker, D.L. Cho, P.M. Claesson, J. Phys. Chem. 93 (1989) 6121.
67. H.K. Christenson, P.M. Claesson, J. Berg, P. C. Herder, J. Phys. Chem. 93 (1989) 1472.
68. K. Kurihara, S. Kato, T. Kunitake, Chem. Lett. (Chem. Soc. Japan), 1555-1558.
69. H.K. Christenson, J. Fang, B.W. Ninham, J.L. Parker, J. Phys. Chem. 94 (1990) 8004.
70. H.K. Christenson, P.M. Claesson, J.L. Parker, J. Phys. Chem. 96 (1992) 6725.
71. H.K. Christenson, J.L. Parker, V.V. Yaminsky, Langmuir 8 (1992) 2080.
72. J.L. Parker, P.M. Claesson, P. Attard, J. Phys. Chem. 98 (1994) 8468.
73. V.S.J. Craig, B.W. Ninham, R.M. Pashley, Langmuir 14 (1998) 3326.
74. A. Carambassis, L.C. Jonker, P. Attard, M.W. Rutland, Phys. Rev. Lett. 80 (1998) 5357.
75. Z. Xu, R.H. Yoon, J. Colloid Interface Sci. 134 (1990) 427.

76. Z. Zhou, P. Wu, C. Ma, Colloids Surf. 50 (1990) 177.
77. S. Tchaliovska, P. Herder, R. Pugh, P. Stenius, J.C. Eriksson, Langmuir 6, (1990) 1533.
78. C.A. Helm, J.N. Israelachvili, P.M. McGuiggan, Biochemistry 31 (1992) 1794.
79. V.S.J. Craig, B.W. Ninham, R.M. Pashley, Langmuir 15 (1999) 1562.
80. J.C. Eriksson, S. Ljunggren, P.M. Claesson, J. Chem. Soc. Faraday Trans. 2, 85 (1989) 163.
81. W.A. Ducker, Z. Xu, J.N. Israelachvili, Langmuir 10 (1994) 3279.
82. P. Attard, Langmuir 12 (1996) 1693.
83. V.V. Yaminsky, Colloids Surf. A 129 (1997) 415.
84. J. Mahnke, J. Stearnes, R.A. Hayes, D. Fornasiero, J. Ralston, Phys. Chem. Chem. Phys. 1 (1999) 2793.
85. R.F. Considine, R.A. Hayes, R.G. Horn, Langmuir 15 (1999) 1657.
86. R.F. Considine, C. Drummond, Langmuir 16 (2000) 631.
87. P. Attard, Langmuir 16 (2000) 4455.
88. N. Ishida, T. Inoue, K. Higashitani, Langmuir 16 (2000) 6377.
89. P.H. Elworthy, A.T. Florence, J.A. Rogers, J. Colloid Interface Sci. 35 (1971) 23.
90. D. Exerowa, M. Zacharieva, R. Cohen, D. Platikanov, Colloid Polym. Sci. 257 (1979) 1089.
91. O.D. Velev, T.D. Gurkov, S.K. Chakarova, B. Dimitrova, I.B. Ivanov, R.P. Borwankar, Colloids Surf. 83 (1994) 43.
92. K. Marinova, R. Alargova, N. Denkov, O. Velev, D. Petsev, I.B. Ivanov, R.P. Borwankar, Langmuir 12 (1996) 2045.
93. I. Langmuir, J. Chem. Phys. 6 (1938) 873.
94. V.M. Muller, Kolloidn. Zh. 38 (1976) 704.
95. J.N. Israelachvili, G.E. Adams, J. Chem. Soc. Faraday Trans. 1, 74 (1978) 975.
96. J.N. Israelachvili, R.M. Pashley, Nature 300 (1982) 341.
97. R.M. Pashley, J. Colloid Interface Sci. 80 (1981) 153.
98. R.M. Pashley, J. Colloid Interface Sci. 83 (1981) 531.
99. J.N. Israelachvili, H. Wennerström, J. Phys. Chem. 96 (1992) 520.
100. V.N. Paunov, R.I. Dimova, P.A. Kralchevsky, G. Broze, A. Mehreteab, J. Colloid Interface Sci. 182 (1996) 239.
101. S. Marčelja, N. Radič, Chem. Phys Lett. 42 (1976) 129.
102. B. Jönsson, H. Wennerström, J. Chem. Soc., Faraday Trans. 2, 79 (1983) 19.
103. S. Leikin, A.A. Kornyshev, J. Chem. Phys. 92 (1990) 6890.
104. D. Henderson, M. Lozada-Cassou, J. Colloid Interface Sci. 114 (1986) 180; ibid. 162 (1994) 508.
105. S. Basu, M.M. Sharma, J. Colloid Interface Sci. 165 (1994) 355.
106. T.W. Healy, A. Homolam, R.O. James, R.J. Hunter, Faraday Discuss. Chem. Soc. 65 (1978) 156.
107. J.J. Bikerman, Philos. Mag. 33 (1942) 384.

108. J. S. Rowlinson, Development of Theories of Inhomogeneous Fluids", in: "Fundamentals of Inhomogeneous Fluids", D. Henderson (Ed.), Marcel Dekker, New York, 1992.
109. P. Claesson, A.M. Carmona-Ribeiro, K. Kurihara, J. Phys. Chem. 93 (1989) 917.
110. R.G. Horn, D.T. Smith, W. Haller, Chem. Phys. Lett., 162 (1989) 404.
111. P. Debye, E. Hückel, Z. Phys. 24 (1923) 185.
112. P. Debye, E. Hückel, Z. Phys. 24 (1923) 305.
113. R.A. Robinson, R.H. Stokes, "Electrolyte Solutions", Butterworths, London, 1959.
114. T.L. Hill, "An Introduction to Statistical Thermodynamics", Addison-Wesley, Reading, MA, 1962.
115. L.D. Landau, E.M. Lifshitz, Statistical Physics, Part 1; Pergamon Press, Oxford, 1980.
116. L. Guldbrand, B. Jönsson, H. Wennerström, P. Linse, J. Chem. Phys. 80 (1984) 2221.
117. H. Wennerström, B. Jönsson, P. Linse, J. Chem. Phys. 76 (1982) 4665.
118. R. Kjellander, S. Marčelja, J. Phys. Chem. 90 (1986) 1230.
119. P. Attard, D.J. Mitchell, B.W. Ninham, J. Chem. Phys., 89 (1988) 4358.
120. P.A. Kralchevsky, V.N. Paunov, Colloids Surf. 64 (1992) 245.
121. J. K. Angarska, K.D. Tachev, P.A. Kralchevsky, A. Mehreteab, G. Broze, J. Colloid Interface Sci. 200 (1998) 31.
122. J.A. de Feijter, A. Vrij, J. Colloid Interface Sci., 70 (1979) 456.
123. R. Kjellander, S. Marčelja, Chem. Phys. Lett., 112 (1984) 49.
124. P. Richmond, J. Chem. Soc. Faraday Trans. 2, 70 (1974) 1066.
125. M.J. Grimson, P. Richmond, C.S. Vassilieff, in: "Thin Liquid Films", I.B. Ivanov (Ed.), Marcel Dekker, New York, 1988; p. 298.
126. J. Marra, J. Phys. Chem. 90 (1986) 2145.
127. J. Marra, Biophys. J. 50 (1986) 815.
128. R. Kjellander, S. Marčelja, R.M. Pashley, J.P. Quirk, J. Phys. Chem. 92 (1988) 6489.
129. R. Kjellander, S. Marčelja, R.M. Pashley, J.P. Quirk, J. Chem. Phys. 92 (1990) 4399.
130. A. Khan, B. Jönsson, H. Wennerström, J. Phys. Chem. 89 (1985) 5180.
131. M.M. Kohonen, M.E. Karaman, R. M. Pashley, Langmuir 16 (2000) 5749.
132. A.D. Nikolov, D.T. Wasan, J. Colloid Interface Sci. 133 (1989) 1.
133. A.D. Nikolov, P.A. Kralchevsky, I.B. Ivanov, D.T. Wasan, J. Colloid Interface Sci. 133 (1989) 13.
134. A.D. Nikolov, D.T. Wasan, N.D. Denkov, P.A. Kralchevsky, I.B. Ivanov, Prog. Colloid Polym. Sci. 82 (1990) 87.
135. D.T. Wasan, A.D. Nikolov, P.A. Kralchevsky, I.B. Ivanov, Colloids Surf. 67 (1992) 139.
136. S. Asakura, F. Oosawa, J. Chem. Phys. 22 (1954) 1255.
137. S. Asakura, F. Oosawa, J. Polym. Sci. 33 (1958) 183.
138. H. de Hek, A. Vrij, J. Colloid Interface Sci. 84 (1981) 409.
139. I. K. Snook, W. van Megen, J. Chem. Phys. 72 (1980) 2907.
140. R. Kjellander, S. Marčelja, Chem. Phys Lett. 120 (1985) 393.
141. P. Tarazona, L. Vicente, Mol. Phys. 56 (1985) 557.

142. E.S. Johnnott, Phil. Mag. 70 (1906) 1339.
143. R.E. Perrin, Ann. Phys. 10 (1918) 160.
144. H.G. Bruil, J. Lyklema, Nature 233 (1971) 19.
145. S. Friberg, St. E. Linden, H. Saito, Nature 251 (1974) 494.
146. J.W. Keuskamp, J. Lyklema, ACS Symp. Ser. 8 (1975) 191.
147. P.M. Kruglyakov, Kolloidn. Zh. 36 (1974) 160.
148. P.M. Kruglyakov, Yu. G. Rovin, "Physical Chemistry of Black Hydrocarbon Films", Nauka, Moscow, 1978 [in Russian].
149. K.G. Marinova, T.D. Gurkov, T.D. Dimitrova, R.G. Alargova, D. Smith, Langmuir 14 (1998) 2011.
150. C.D. Dushkin, K. Nagayama, T. Miwa, P.A. Kralchevsky, Langmuir 9 (1993) 3695.
151. E. Manev, S.V. Sazdanova, D.T. Wasan, J. Dispersion Sci. Technol. 5 (1984) 111.
152. P.A. Kralchevsky, A.D. Nikolov, D.T. Wasan, I.B. Ivanov, Langmuir 6 (1990) 1180.
153. K. Koczo, A.D. Nikolov, D.T. Wasan, R.P. Borwankar, A. Gonsalves, J. Colloid Interface Sci. 178 (1996) 694.
154. G.N. Sethumadhavan, A.D. Nikolov, D.T. Wasan, Langmuir 17 (2001) 2059.
155. E.S. Basheva, K.D. Danov, P.A. Kralchevsky, Langmuir 13 (1997) 4342.
156. V. Bergeron, and C. J. Radke, Langmuir 8 (1992) 3020.
157. P. Richetti, P. Kékicheff, Phys. Rev. Lett. 68 (1992) 1951.
158. J.L. Parker, P. Richetti, P. Kékicheff, S. Sarman, Phys. Rev. Lett. 68 (1992) 1955.
159. O. Krichevsky, J. Stavans, Phys. Rev. Lett. 74 (1995) 2752.
160. D. Henderson, J. Colloid Interface Sci. 121 (1988) 486.
161. D.T. Mitchell, B.W. Ninham, B.A. Pailthorpe, J. Chem. Soc. Faraday Trans. II, 74 (1978) 1116.
162. R. Kjellander, S. Sarman, Chem. Phys. Lett. 149 (1988) 102.
163. P. Attard, J.L. Parker, J. Phys. Chem. 96 (1992) 5086.
164. M. L. Pollard, and C. J. Radke, J. Chem. Phys. 101 (1994) 6979.
165. G. Karlström, Chem. Scripta 25 (1985) 89.
166. X.L. Chu, A.D. Nikolov, D.T. Wasan, Langmuir 10 (1994) 4403.
167. X.L. Chu, A.D. Nikolov, D. T. Wasan, J. Chem. Phys. 103 (1995) 6653.
168. P.A. Kralchevsky, N.D. Denkov, Chem. Phys. Lett. 240 (1995) 385; Prog. Colloid Polymer Sci. 98 (1995) 18.
169. N.F. Carnahan, K.E. Starling, J. Chem. Phys. 51 (1969) 635.
170. N.A. Mazer, Chapter 8 in: "Dynamic Light Scattering", R. Pecora (Ed.), Plenum Press, London, 1985.
171. P.N. Pusey, Chapter 2 in: "Dynamic Light Scattering", R. Pecora (Ed.), Plenum Press, London, 1985.
172. C. Bondy, Trans. Faraday Soc. 35 (1939) 1093.
173. E. Evans, D. Needham, Macromolecules 21 (1988) 1822.
174. J.F. Joanny, L. Leibler, P.G. de Gennes, J. Polym. Sci. 17 (1979) 1073.

175. P.D. Patel, W.B. Russel, J. Colloid Interface Sci. 131 (1989) 192.
176. M.P. Aronson, Langmuir 5 (1989) 494.
177. B. van Lent, R. Israels, J. Scheutjens, G. Fleer, J. Colloid Interface Sci. 137 (1990) 380.
178. T.L. Kuhl, A.D. Berman, J.N. Israelachvili, Macromolecules 31 (1998) 8250.
179. T.L. Kuhl, A.D. Berman, J.N. Israelachvili, Macromolecules 31 (1998) 8258.
180. Th. F. Tadros, Steric Interactions in Thin Liquid Films", in: "Thin Liquid Films", I.B. Ivanov (Ed.), Marcel Dekker, New York, 1988, p. 331.
181. S.S. Patel, M. Tirel, Ann. Rev. Phys. Chem. 40 (1989) 597.
182. H.J. Ploehn, W.B. Russel, Adv. Chem. Eng., 15 (1990) 137.
183. P.G. de Gennes, "Scaling Concepts in Polymer Physics", Cornel Univ. Press, Ithaca, NY, 1979; Chap. III.1.
184. A.K. Dolan, S.F. Edwards, Proc. Roy. Soc. (London) A337 (1974) 509.
185. A.K. Dolan, S.F. Edwards, Proc. Roy. Soc. (London) A343 (1975) 627.
186. S.J. Alexander, Physique 38 (1977) 983.
187. P.G. de Gennes, C. R.. Acad. Sci. (Paris) 300 (1985) 839.
188. P.G. de Gennes, Adv. Colloid Interface Sci., 27 (1987) 189.
189. H.J. Taunton, C. Toprakcioglu, L.J. Fetters, J. Klein, Macromolecules 23 (1990) 571.
190. P.M. Claesson, R. Kjellander, P. Stenius, H.K. Christenson, J. Chem. Soc. Faraday Trans. I, 82 (1986) 2735.
191. W. Helfrich, Z. Naturforsch. 33a (1978) 305.
192. R.M. Servuss, W. Helfrich, J. Phys. (France) 50 (1989) 809.
193. L. Fernandez-Puente, I. Bivas, M.D. Mitov, P. Méléard, Europhys. Lett. 28 (1994) 181.
194. C.R. Safinya, D. Roux, G.S. Smith, S.K. Sinha, P. Dimon, N.A. Clark, A.M. Bellocq, Phys. Rev. Lett. 57 (1986) 2718.
195. T.J. McIntosh, A.D. Magid, S.A. Simon, Biochemistry 28 (1989) 7904.
196. O. Abillon, E. Perez, J. Phys. (France) 51 (1990) 2543.
197. H. Bagger-Jörgensen, U. Olsson, Langmuir 12 (1996) 4057.
198. D.A. Antelmi, P. Kékicheff, J. Phys. Chem. B, 101 (1997) 8169.
199. J.Y. Walz, E. Ruckenstein, J. Phys. Chem. B, 103 (1999) 7461.
200. J.-P. Douliez, A. Léonard, E.J. Dufourc, J. Phys. Chem. 100 (1996) 18450.
201. J. Majewski, T.L. Kuhl, K. Kjaer, M.C. Gerstenberg, J. Als-Nielsen, J.N. Israelachvili, G.S. Smith, J Amer. Chem. Soc. 120 (1998) 1469.
202. G.A.E. Aniansson, S.N. Wall, M. Almgren, H. Hoffman, I. Kielmann, W. Ulbricht, R. Zana, J. Lang, C. Tondre, J. Phys. Chem. 80 (1976) 905.
203. G.A.E. Aniansson, J. Phys. Chem. 82 (1978) 2805.